The correlated basis function approach

Alessandro Lovato

June 19, 2017

1 Ab initio approaches

Ab initio nuclear many-body approaches are based on the premise that nuclear dynamics can be modeled studying exactly solvable systems. This is a most important feature since, due to the complexity of strong interactions and to the prohibitive difficulties associated with the solution of the quantum mechanical many-body problem, theoretical calculations of nuclear observables generally involve a number of approximations. Hence, models of nuclear dynamics extracted from analyses of the properties of complex nuclei are plagued by the systematic uncertainties associated with the use of a specific approximation scheme.

In nuclear many-body theory nucleons are treated as point like non relativistic particles, the dynamics of which are described by the Hamiltonian

$$H = \sum_{i=1}^{A} \frac{\mathbf{p}_i^2}{2m} + \sum_{j>i=1}^{A} v_{ij} + \sum_{k>j>i=1}^{A} V_{ijk} \ . \tag{1}$$

In the above equation, $\mathbf{p}_i$ is the momentum of the i-th nucleon, while the potentials v_{ij} and V_{ijk} describe two- and three-nucleon interactions, respectively.

The nucleon-nucleon (NN) potential is obtained from an accurate fit to the available data on the two-nucleon system, in both bound and scattering states, and reduces to the Yukawa one-pion-exchange potential at large distances. State-of-the-art parameterizations of v_{ij}, both phenomenological and derived within chiral perturbation theory [1, 2, 3, 4], are written in the form

$$v_{ij} = \sum_{n=1}^{18} v^n(r_{ij}) O_{ij}^n \ , \tag{2}$$

with $r_{ij} = |\mathbf{r}_i - \mathbf{r}_j|$ and

$$O_{ij}^{n\leq 6} = [1, (\boldsymbol{\sigma}_i \cdot \boldsymbol{\sigma}_j), S_{ij}] \otimes [1, (\boldsymbol{\tau}_i \cdot \boldsymbol{\tau}_j)] \ , \tag{3}$$

where $\boldsymbol{\sigma}_i$ and $\boldsymbol{\tau}_i$ are Pauli matrices acting in spin and isospin space, respectively, and

$$S_{ij} = \frac{3}{r_{ij}^2}(\boldsymbol{\sigma}_i \cdot \mathbf{r}_{ij})(\boldsymbol{\sigma}_j \cdot \mathbf{r}_{ij}) - (\boldsymbol{\sigma}_i \cdot \boldsymbol{\sigma}_j) \ . \tag{4}$$

is the tensor operator. The operators corresponding to $n = 7, \ldots, 14$ are associated with the non static components of the NN interaction, while those corresponding to $p = 15, \ldots, 18$ account for small violations of charge symmetry. Being fit to the full Nijmegen phase-shift database, as well as to low energy scattering parameters and deuteron properties, the Argonne v_{18} potential provides an accurate description of the two-nucleon system by construction.

The inclusion of the additional three-body term, V_{ijk}, is needed to explain the binding energies of the three-nucleon systems [5]. The derivation of V_{ijk} was first discussed in the pioneering work of Fujita and Miyazawa [6], who argued that its main contribution originates from the two-pion exchange process in which a NN interaction leads to the excitation of one of the participating particles to a Δ resonance, which then decays in the aftermath of the interaction with a third nucleon.

Commonly used models of the three-nucleon potential are written in the form

$$V_{ijk} = V_{ijk}^{2\pi} + V_{ijk}^{N} \ , \tag{5}$$

where $V_{ijk}^{2\pi}$ is the attractive Fujita-Miyazawa term, while V_{ijk}^{N} is a purely phenomenological repulsive term. The parameters entering the definition of the above potential are adjusted in such a way as to reproduce the ground state energy of the three-nucleon systems.

Nuclear ab initio approaches are aimed at solving the time-independent Schrödinger equation

$$\hat{H}\Psi_n(x_1, \ldots, x_A) = E_n\Psi_n(x_1, \ldots, x_A) \tag{6}$$

for the Hamiltonian defined in Eq.(1) without any additional adjustable parameters.

In the first Section of this notes we discuss the independent particle model, and argue that it is not suitable to encompass correlation structure induced by the nuclear Hamiltonian. The following Sections are devoted to more advanced approaches, allowing one to take into account correlation effects. We will focus on the variational method, based on correlated basis function (CBF) theory, and the diffusion Monte Carlo technique.

2 Mean field approach: the Hartree-Fock method

D. R. Hartree [7], V. A. Fock [8] and J. C. Slater [9], proposed to use as a starting point toward the solution of the many-body Schroedinger equation describing atomic electrons, the *central field approximation*. Within this approximation, based on the *independent particle model*, each nucleon moves in a single-particle effective potential representing the average effect of the interactions with the other $A-1$ nucleons. Each nucleon is described by its own

wave function, $\phi_{n_i}(x_i)$ eigenfunction of the hermitian operator $\hat{h}^{HF}$

$$\hat{h}^{HF}(x_i)\phi_{n_i}(x_i) = \epsilon_{n_i}\phi_{n_i}(x_i)\,, \tag{7}$$

where the generalized coordinate $x_i = \{\mathbf{r}_i, \sigma_i, \tau_i\}$ represents both the position and the spin-isospin variables of the i-th nucleon. The operator $\hat{h}^{HF}$, denoted as the one-particle Fock Hamiltonian, is given by

$$\hat{h}^{HF}(x_i) = -\frac{\nabla_i^2}{2m} + \hat{v}^{HF}(x_i)\,, \tag{8}$$

where $\hat{v}^{HF}(r)$ is the single particle Hartree-Fock potential, that is built from the states $\phi_{n_i}(x_i)$ using a *self-consistent* iterative procedure, based on the variational principle, described in Appendix A. Within this approximation, the many particle ground-state for a system made of A nucleons is a single Slater determinant of single-nucleon states

$$\Phi_0 = \mathcal{A}[\phi_{n_1}(x_1)\ldots\phi_{n_A}(x_A)]\,. \tag{9}$$

where $\mathcal{A}$ is the antisymmetrization operator.

As shown in Appendix A, the *single particle energy* ϵ_i is given by

$$\epsilon_{n_i} = \frac{\mathbf{k}_i^2}{2m} + \sum_{n_j=1}^{A}\int dx_i dx_j \phi^*_{n_i}(x_i)\phi^*_{n_j}(x_j)\hat{v}_{ij}[\phi_{n_i}(x_i)\phi_{n_j}(x_j) - \phi_{n_j}(x_i)\phi_{n_i}(x_j)]\,, \tag{10}$$

where $\int dx_j$ stands for integration over the coordinate $\mathbf{r}_j$ and trace over the spin and isospin variables of the j–th nucleon. The total energy of the system, $E[\Phi_0]$, is *not* the sum of the single particle energies, rather

$$E[\Phi_0] = \sum_{n_i}\epsilon_{n_i} - \frac{1}{2}\sum_{n_i,n_j}\int dx_j \phi^*_{n_i}(x_i)\phi^*_{n_j}(x_j)\hat{v}_{ij}[\phi_{n_i}(x_i)\phi_{n_j}(x_j) - \phi_{n_j}(x_i)\phi_{n_i}(x_j)]\,. \tag{11}$$

A physical meaning to the single particle energies can be given through *Koopmans' theorem*. Assuming that the spin orbitals of the $A-1$ system are the same as those of the A system, from the previous equation it can be shown that ϵ_{n_i} is the *separation energy* of the nucleon in the state ϕ_{n_i}

$$\epsilon_{n_i} = E_A - E_{A-1}(i)\,. \tag{12}$$

The self-consistent field method allows for the determination of the spin-orbitals of the A occupied states, $\{\phi_1,\ldots,\phi_A\}$, with single-particle energies $\epsilon_1,\ldots,\epsilon_A$, E_A being the Fermi energy of the system. The remaining eigenfunctions of $\hat{h}^{HF}$, which satisfy Eq. (191), are associated with unoccupied (virtual) states having single particle energies larger than the Fermi energy. Unlike $\{\phi_1,\ldots,\phi_A\}$, they are not determined in a self-consistent fashion, as they do not enter the definition of the Fock Hamiltonian.

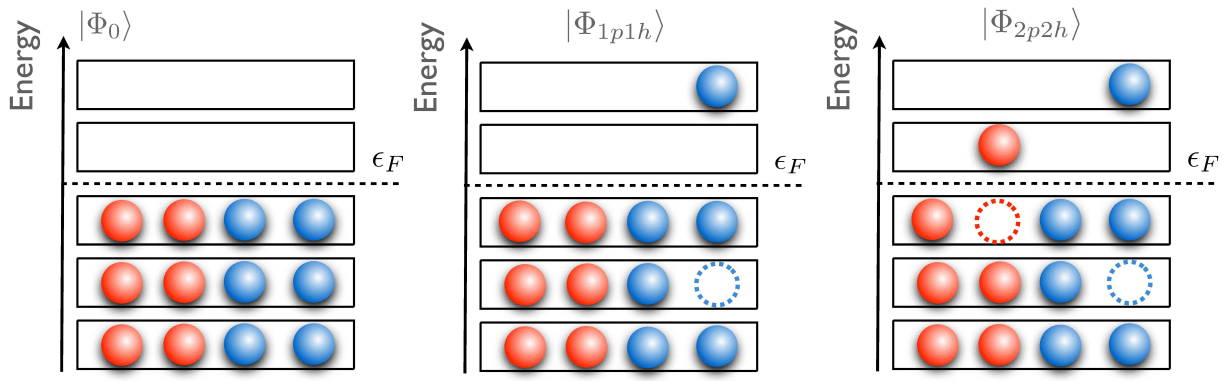

Figure 1: Schematic representation of the ground, 1p-1h, and 2p-2h states.

The key point of the Hartree Fock approach is that occupied and virtual states provide a natural basis to describe the many-body system [10]. While the many-body ground state of Eq. (9) is the Slater determinant of occupied single-particle states excited many-body states are constructed by removing n occupied states from the Slater determinant and replacing them with n virtual states. Such excited states, schematically represented in Fig. 1, are called n-particle n-hole (np-nh) states and are eigenstates of the Hartree Fock Hamiltonian

$$\hat{H}^{HF} = \sum_{i=1}^{A} \hat{h}_i^{HF}$$

$$\hat{H}^{HF}|\Phi_{h_1,\ldots,h_n;p_1,\ldots,p_n}\rangle = \Big[\sum_{n_i=1}^{A} \epsilon_{n_i} + \sum_{i=1}^{n}(\epsilon_{p_i} - \epsilon_{h_i})\Big]|\Phi_{h_1,\ldots,h_n;p_1,\ldots,p_n}\rangle\,. \tag{13}$$

The Hartree-Fock procedure is the basis, for instance, of the nuclear shell model, that has been successfully applied to explain many nuclear properties. [11, 12, 13]. As far as nuclear matter is concerned, the single particle wave functions are known to be plane waves, as dictated by translation invariance. Therefore, a uniform system can be conveniently described within a box of volume V with periodic boundary conditions [14], using the wave functions

$$\phi_{n_i}(x_i) = \frac{e^{i\mathbf{k}_i\cdot\mathbf{r}_i}}{\sqrt{V}}\eta_{\alpha_i}\,, \tag{14}$$

where $\eta_{\alpha_i} \equiv \chi_{\sigma_i}\chi_{\tau_i}$ represents the product of Pauli spinors describing the spin and the isospin of particle i. In order to satisfy the periodic boundary conditions, the wave vector $\mathbf{k}$ is discretized; for a cubic box of side L, it turns out that

$$k_i = \frac{2\pi}{L}n_i \qquad i = x, y, z \qquad n_i = 0, \pm1, \pm2, \ldots\,. \tag{15}$$

The momentum of the occupied states is smaller than the Fermi momentum $\mathbf{k}_F$, which is related to the density of the system, ρ, through $k_F = (6\pi^2\rho/\nu)^{1/3}$, and ν is the spin-isospin

degeneracy ($\nu = 2$ for pure neutron matter (PNM), $\nu = 4$ for symmetric nuclear matter (SNM)).

The plane waves of Eq. (14) are already solutions to the Hartree Fock equations; in other words they are the best single-particle wave functions for uniform systems. A remarkable feature of nuclear matter is that the starting single particle wave functions are known and simple, unlike what happens, for instance, in finite nuclei. Due to the lack of translation invariance, even generating the single particle wave functions is a difficult task, as it requires the solution of the Hartree-Fock equations [14].

The single particle energy of nuclear matter can be easily derived substituting the wave function of Eq. (14) in Eq. (10). In the case of SNM ($\nu = 4$) for potentials of the form of Argonne v_{18}, carrying out the summation over the occupied states with $|\mathbf{k}_j| \leq k_F$ yields

$$\epsilon_{n_i} = \frac{\mathbf{k}_i^2}{2m} + \rho \int d\mathbf{r}_{ij} \Big[v_{ij}^c - \frac{1}{4} \ell(k_F r_{ij}) e^{-i\mathbf{k}_i \cdot \mathbf{r}_{ij}} (v_{ij}^c + 3v_{ij}^\tau + 3v_{ij}^\sigma + 9v_{ij}^{\sigma\tau}) \Big] . \tag{16}$$

where the Slater function is given by

$$\ell(k_F r) = 3 \Big[\frac{\sin(k_F r) - 3k_F r \cos(k_F r)}{(k_F r)^3} \Big] . \tag{17}$$

Summing over spin-isospin states of Eq. (10) amounts to tracing over the spin-isospin variables of the nucleon j. Such a trace is normalized, as it incorporates the factor $1/\nu$ coming from the summation over the momentum $\mathbf{k}_j$. The factor A arising from the same sum, divided by wave function normalization factor V produces the factor ρ, appearing in Eq. (16).

Standard perturbation theory performed in the basis of the Hartree-Fock solutions can not cope with the repulsive core and the strong tensor component of the nuclear force, which cause individual terms of the perturbative expansion to diverge [15]. As an example [16], consider the scalar repulsive potential

$$v(\mathbf{r}) = \begin{cases} |v_0| & |\mathbf{r}| \leq r_0 \\ 0 & |\mathbf{r}| > r_0 \, . \end{cases} \tag{18}$$

The single particle energy computed from Eq. (16) using this potential is seen to be of order $\rho \, r_0^3 |v_0|$; if the potential approaches the hard sphere interaction, similar to the strong repulsive core of the nuclear interaction, the single particle energy keeps increasing.

In other words, since the eigenfunctions of the Fock Hamiltonian are the same as those of the non interacting Fermi gas, the many-body wave function largely differs from the exact ground state associated with the nuclear Hamiltonian. Standard perturbation theory in such a basis can not be expected to be convergent as the matrix elements of the nuclear Hamiltonian between np-nh states are not perturbative corrections to the ground state expectation value.

The two main avenues to overcome the above problem are based either on the replacement of the bare nucleon-nucleon potential with an effective interaction, or on the use of a basis of *correlated* states, embodying non-perturbative interaction effects [17, 18].

Within the former approach proposed by Brueckner [19, 20, 21, 22], the bare potential v_{ij}, is replaced by a well behaved effective interaction, the G-matrix, which is obtained by summing up the series of particle-particle ladder diagrams. The physical basis of this theory was elucidated by Bethe [23], while Goldstone introduced the linked cluster expansion [24]. For a more recent review of the G-matrix approach, also known as Brueckner-Bethe-Goldstone expansion, see Refs. [25, 26]. In recent years, it has been suggested that effective interactions suitable for perturbative calculations can also be obtained combining potentials derived within chiral perturbation theory and renormalization group evolution to low momentum [27, 28, 29]. This procedure has proven to be particularly successful for the description of medium-mass nuclei and PNM.

The remainder of this note will be devoted to the latter approach: the correlated basis function theory.

3 Correlated basis functions theory

Theories of Fermi liquids based on correlated basis functions are a natural extension of variational approaches in which the trial ground state wave function is written in the form

$$|\Psi_0\rangle = \frac{\hat{\mathcal{F}}|\Phi_0\rangle}{\langle\Phi_0|\hat{\mathcal{F}}^\dagger\hat{\mathcal{F}}|\Phi_0\rangle}, \tag{19}$$

where $\hat{F}$ is suitable many-body correlation operator. The simplest choice suitable for dealing with the strong short-range repulsions is the scalar correlator of the form

$$\hat{\mathcal{F}} = \prod_{j>i=1}^{A} f(r_{ij})\,, \tag{20}$$

known as Jastrow correlator [16]. However, this choice for the correlation operator is only suitable for purely central potentials, such as those describing the interaction between ^{3}He atoms. For state-dependent potentials, like the Argonne nuclear interaction, spin-isospin dependent correlations, to be introduced at a later stage, are needed.

The variational approach consists in the minimization of the expectation value of the Hamiltonian

$$E_V = \langle\Psi_0|\hat{H}|\Psi_0\rangle \tag{21}$$

which is an upper bound to the true ground-state energy: $E_V \geq E_0$. For instance, in the pure central Jastrow case, minimizing E_V allows for finding the radial function $f(r_{ij})$. Apart from the technical difficulties involved in finding the optimal radial function, it is clear that the resulting correlation function is small within the repulsive region of the NN potential. As noted in the review of Clark [17], historically, the development of the variational approach has been somewhat discouraged not only by the difficulties involved in the calculation of

E_V, potentially leading to violations of the variational principle, but also by a psychological obstacle: the embarrassing conceptual simplicity of the method, in other words, its lack of "snob appeal".

Nevertheless, the variational approach succeeded in treating the atomic helium in both the liquid and solid phases [30, 31]. Although nowadays the numerical problem of solving the many-body Schrödinger equation for the ground state has been resolved, to a large extent, by the Green's function Monte Carlo method [32], this approach does not provide a quantitative understanding of the ground-state wave function [33]. However, the knowledge of the analytic form of the ground-state function would be particularly useful to extend the microscopic theory to treat the elementary excitations and finite-temperature properties of helium liquids. A successful approach in this direction has been provided by the variational theory [34], including also the *back flow correlation*, proposed by Feynman and Cohen [35]: a velocity dependent correlation, arising from the flow induced by a moving atom.

As far as the nuclear many body problem in concerned, a number variety of experimental evidence [36, 37] showing that short-range NN correlations are a fundamental feature of nuclear structure. The description of nuclear dynamics in terms of interactions derived in coordinate space appears to be the most appropriate, for both conceptual and technical reasons. First of all, correlations between nucleons are predominantly of spatial nature, in analogy with what happens in all known strongly correlated systems, like liquid ^{4}He. In addition, one needs to clearly distinguish the effects due to the short-range repulsion from those due to relativity.

The correlated basis theories of Fermi liquids are a natural extension of the variational approach. A non orthogonal but complete set of correlated basis states can be defined as [38, 39]

$$|\Psi_n\rangle \equiv \frac{\hat{\mathcal{F}}|\Phi_n\rangle}{\langle\Phi_n|\hat{\mathcal{F}}^\dagger\hat{\mathcal{F}}|\Phi_n\rangle}, \tag{22}$$

where $|\Phi_n\rangle$ is the n-p n-h state of Eq. (13). The correlation operator,$\hat{\mathcal{F}}$, is determined by the variational calculation of the ground state energy. The variational energies E_n^v, although only E_0^v has been variationally estimated, are given by the diagonal matrix elements of the Hamiltonian between correlated states

$$E_n^v = \langle\Psi_n|\hat{H}|\Psi_n\rangle\,. \tag{23}$$

The energies E_n^v are extensive quantities, as they are of order A, while excitation energies $E_n^v - E_0^v$ are of order 1.

In order to compute the perturbative corrections to the variational energies, the Hamiltonian H is decomposed in two terms

$$\hat{H} = \hat{H}^0 + \hat{H}^1\,. \tag{24}$$

where, as will became clear in the following, neither $\hat{H}_0$ nor $\hat{H}_1$ are hermitian operators. The "unperturbed" Hamiltonian $\hat{H}^0$ is defined through the correlated basis states and the

variational energies, in such a way that

$$\hat{H}^0|\Psi_n\rangle = E_n^v|\Psi_n\rangle \tag{25}$$

Notice that, since the correlated states are not orthogonal, $\hat{H}^0$ is not diagonal in this basis

$$\langle\Psi_n|\hat{H}^0|\Psi_m\rangle = E_m^v N_{nm}\,. \tag{26}$$

The metric matrix N_{nm} is defined by

$$N_{nm} \equiv \delta_{nm} + S_{nm} \equiv \langle\Psi_n|\Psi_m\rangle\,, \tag{27}$$

where S_{nm} is the overlap matrix, with

$$S_{nn} = 0\,. \tag{28}$$

It is convenient to distinguish the diagonal and the non-diagonal matrix elements of the Hamiltonian

$$H_{nm} \equiv \langle\Psi_n|\hat{H}|\Psi_m\rangle = E_m^v\delta_{nm} + H'_{nm}\,, \tag{29}$$

where $H'_{mm} = 0$. The closer the CBF states are to the true eigenstates of the Hamiltonian, the smaller H'_{nm} becomes. Using Eq. (26) and (27) it turns out that the off-diagonal part of the Hamiltonian matrix element is

$$H'_{nm} = E_m^v S_{nm} + H^1_{nm}\,, \tag{30}$$

which is consistent with $H^1_{nn} = 0$, resulting from Eqs. (23),(24) and (27).

Assuming that the non-diagonal elements of both the metric and the Hamiltonian be small, there have been two fundamental ways of treating the problem pertubatively. One way, consists in diagonalizing H_{nm} as it is, without bothering to orthogonalize the basis, using the *nonorthogonal perturbation theory*. The other way is employing some procedure to orthogonalize the basis first, and then apply the standard perturbation theory.

Within the former approach, the authors of Ref. [40], by introducing the so called *diagonal metric*, were able to show that the perturbative corrections to the variational energy E_n^v can be casted in a way that is formally identical to standard perturbation theory in an orthogonal basis

$$\begin{aligned} E_n - E_v^n =& V_{nn} + \sum_{k\neq n}\frac{V_{nk}V_{kn}}{E_n^v - E_k^v} + \\ & \Big(\sum_{k\neq n, m\neq n}\frac{V_{nm}V_{mk}V_{kn}}{(E_n^v - E_m^v)(E_n^v - E_k^v)} - V_{nn}\sum_{k\neq n}\frac{V_{nk}V_{kn}}{(E_k^v - E_n^v)^2}\Big) + \ldots \end{aligned} \tag{31}$$

where E_n is the exact eigenvalue of the full Hamiltonian $\hat{H}$. The differences with respect to the orthogonal case are enclosed in the matrix V_{nm}, the perturbative expansion of which reads

$$V_{nm} = (H'_{nm} - S_{nm}E^v_n) - \sum_k S_{nk}(H'_{km} - S_{km}E^v_n) + \sum_{k,l} S_{nk}S_{kl}(H'_{lm} - S_{lm}E^v_n) + \dots . \quad (32)$$

Replacing V_{nm} in Eq. (31) with its expansion leads to

$$E_n - E^n_v = \sum_{k\neq n} \frac{(H'_{nk} - E_nS_{nk})(H'_{kn} - E_nS_{kn})}{E^v_n - E^v_k} + \dots \quad (33)$$

Earlier derivations of the latter result, not involving the diagonal metric formalism, can be found in Refs. [41, 42]. Like in ordinary many-body perturbation theory, each order of the perturbative expansion diverges with the number of particle, A. However in Ref. [43] it has been shown that divergent terms appearing at different orders cancel each other. A major difference with respect to ordinary many-body perturbation theory is that the energy-dependence of the matrix elements V_{nm} of Eq. (31), arising from the non orthogonality of the CBF state. Another peculiar feature of CBF perturbation theory is the fact that V_{nm} is a many-body operator, as, through $\hat{F}$, it incorporates the effect of the correlations among all the particles of the system.

In the earlier calculations [44, 45], where the correlator was taken to be of the simple Jastrow form of Eq. (20), the second order term of the perturbative corrections has been found to be large. As shown in Fig. 2, the NN potential has indeed a non trivial spin-isospin structure, that can not be encompassed only considering pure central correlations. In particular, since this wave function is spherically symmetric, the expectation value of the tensor component of the NN interaction averages to zero. In the pure Jastrow case, the CBF states are not sufficiently close to the exact eigenstates of the Hamiltonian, and many terms in the perturbative series need to be calculated. In liquid ^{3}He or in electron gas, where the potential is purely central, the central Jastrow CBF is much more justified [46].

A generalization of the Jastrow correlation operator whose structure reflects the complexity of the NN interaction has been proposed in Ref. [47, 48, 49]

$$\hat{\mathcal{F}} = \left(\mathcal{S} \prod_{j>i=1}^{A} \hat{F}_{ij}\right) , \quad (34)$$

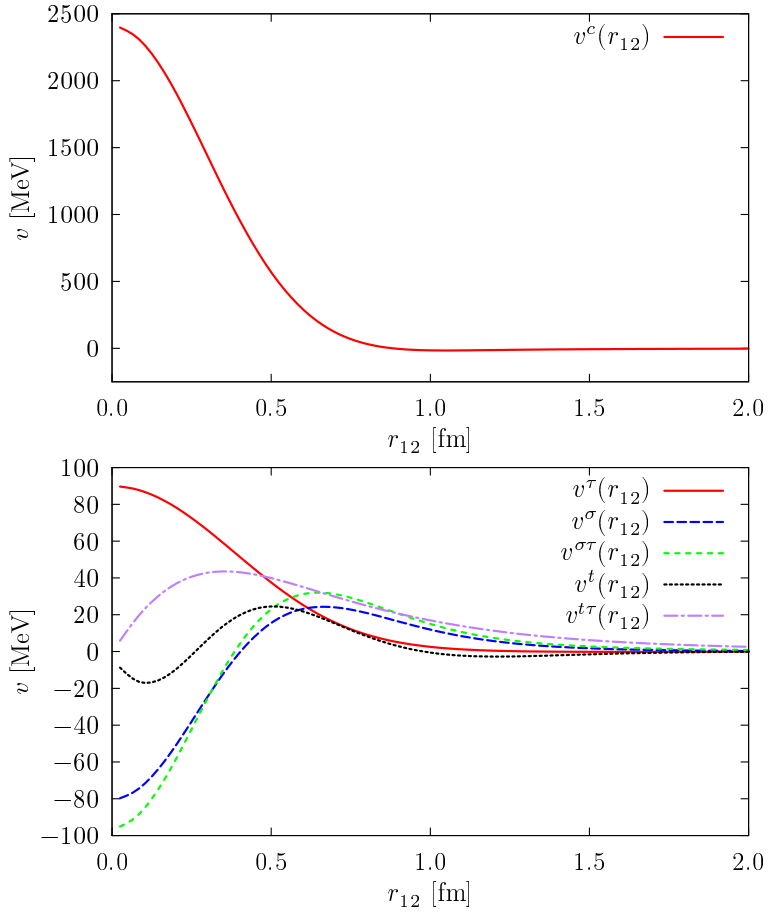

Figure 2: Central (upper panel) and spin-isospin radial functions of the Argonne v_{18} NN potential.

with

$$\hat{F}_{ij} = \sum_{p=1}^{6} f^p(r_{ij}) \hat{O}^p_{ij} \ . \tag{35}$$

Note that the symmetrization operator $\mathcal{S}$ is needed to fulfill the requirement of antisymmetrization of the state $|\Psi_n\rangle$, as in general, $[\hat{O}^p_{ij}, \hat{O}^q_{ik}] \neq 0$.

Since the first six spin-isospin operators of the NN potential form a closed set, this choice for the correlation operator has a tremendous advantage in the analytic manipulations necessary to compute the energy per particle. As will be shown in Section 6, the product of any two of the O^p, $p < 6$, can be reduced to a linear combination of elements from this set. In this lecture notes we will stick to this choice for $\hat{\mathcal{F}}$ although in Ref. [50] the correlation operator has been extended including spin-orbit correlations. In fact, the variational choice of Eq. (35) (F_6 model) implies that spin orbit correlations are neglected. We motivate this choice mainly with the

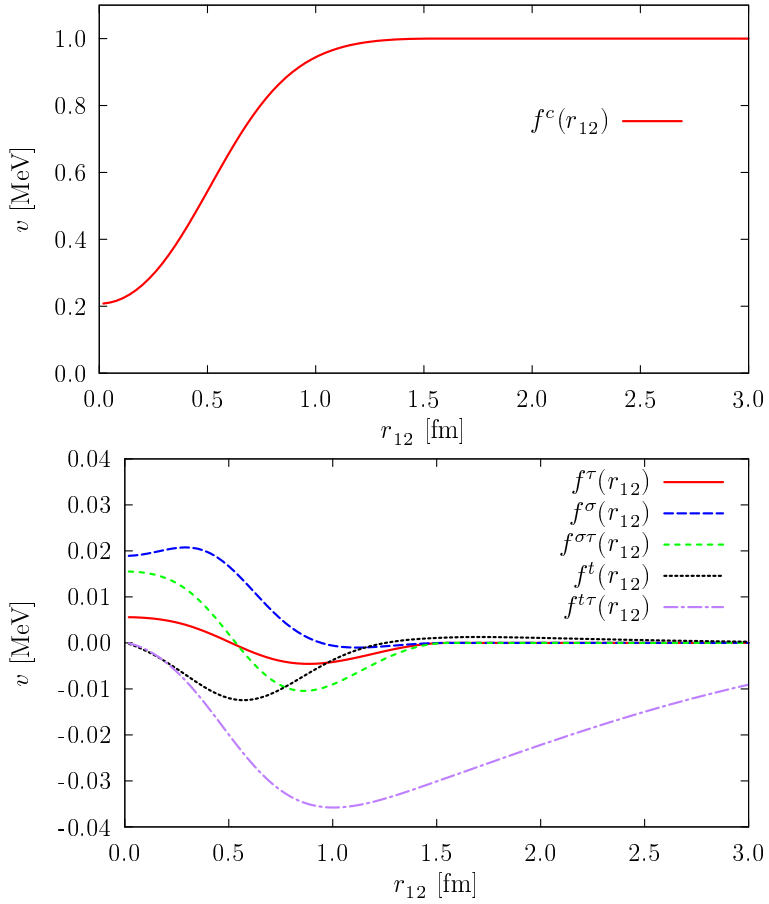

Figure 3: Central (upper panel) and spin-isospin correlation functions for SNM at equilibrium density for the Argonne v_6' plus Urbana IX interaction.

technical difficulties of consistently including spin-orbit correlations; in spite of the calculations performed of Ref. [50], we believe that the contribution of the spin-orbit correlation is still an open problem. In several FHNC/SOC calculations of the binding energy of SNM the spin orbit terms of the potential have been included only pertubatively. Moreover in all the FHNC/SOC calculations of the linear response [51, 52], optical potential and Green's function [53, 54] of SNM, and recent variational Monte Carlo calculations [55], spin-orbit correlations have been neglected.

The correlation operators resulting from the minimization of the energy per particle of SNM at equilibrium density for the Argonne v_6' plus Urbana IX interaction are displayed in Fig. 3. The short-distance behavior is largely shaped by the strongly repulsive core of the NN potential, resulting in a drastic suppression of the probability to find two nucleons at relative distance $r_{ij} \lesssim 1$ fm. At longer distance the non-central, or tensor, components of interaction become prominent.

Before moving to the cluster expansion technique, which has been developed to compute the matrix elements of the Hamiltonian, it is worth spending few words on orthogonal CBF theory. As a matter of fart, a clear analysis of the convergence properties of the non-orthogonal CBF perturbation theory has not been performed yet. For instance, the truncation of the series at some perturbative order leads to non-orthogonality spuriousities, whose effects may not be negligible. Moreover, the calculation of quantities other than the ground-state energy, like the response function, is made difficult by the fact that properly orthogonalized eigenvectors cannot be easily extracted the nonorthogonal CBF basis.

If one attempts to diagonalize the CBF states using the standard Löwdin transformation [56], the resulting states are worst than the original one. For instance, the expectation value of the Hamiltonian in the Löwdin orthogonal ground-state is larger than E_0^v. To avoid this inconvenient, a two-step orthogonalization procedure which preserves the variational diagonal matrix elements of the Hamiltonian and allows for using ordinary orthogonal perturbation theory in zero temperature calculations, has been developed [57].

4 Cluster expansion formalism

The correlation operators of Eq. (20) and (35) are defined in such a way to possess the cluster property. This means that if the system is split in two (or more) subset of particles that are moved far away from each other, the correlation operator factorizes into a product of two (or more) correlation operators in such a way that only particles belonging to the same subset are correlated. For instance, consider two subsets, say $i_1, \dots i_m$ and $i_{m+1}, \dots i_A$; the cluster property implies

$$\hat{\mathcal{F}}(x_1, \dots, x_A) \to \hat{\mathcal{F}}(x_{i_1}, \dots, x_{i_m}) \times \hat{\mathcal{F}}(x_{i_{m+1}}, \dots, x_{i_A}) \,. \tag{36}$$

The above property allows for expanding the matrix elements of the Hamiltonian, (or of any other many-body operator), between CBF states in sum of terms involving an increasing number of particles, knowns as *clusters*. Both analytic [17, 45] and diagrammatic cluster expansion formalisms [58, 59, 60] can be found in the literature; moreover different classification schemes have been adopted, corresponding to different choices for the smallness parameters of the perturbative expansion.

In the calculation of the expectation value of any many-body operator it is convenient to perform separate cluster expansion for the numerator and the denominator, the latter arising from the normalization of CBF states

$$O_{nm} \equiv \langle \Psi_n | \hat{O} | \Psi_m \rangle \equiv \frac{\langle \Phi_n | \hat{\mathcal{F}} \hat{O} \hat{\mathcal{F}} | \Phi_m \rangle}{\langle \Phi_n | \hat{\mathcal{F}} \hat{\mathcal{F}} | \Phi_m \rangle} \equiv \frac{N_{nm}}{D_{nm}} \,. \tag{37}$$

It is a general property of the cluster expansion, to be discussed in detail below, that divergent terms coming from the expansion of the numerator and of denominator cancel.

The two following subsections will be devoted to the description of the original Fantoni Rosati (FR) diagrammatic cluster expansion formalism [58, 59] and to its generalization [61, 18], developed to deal with spin-isospin dependent correlation operators.

5 Fantoni Rosati cluster expansion and FHNC summation scheme

The FR cluster expansion has been obtained through a generalization of the concepts underlying the Mayer expansion scheme, originally developed to describe classical liquids [62], to the case of quantum Bose and Fermi systems. Within the FR approach, both the term $\hat{\mathcal{F}}\hat{H}\hat{\mathcal{F}}$ of the numerator N_{nm} and the term $\hat{\mathcal{F}}\hat{\mathcal{F}}$ of the denominator D_{nm} associated with the expectation value of the Hamiltonian are expanded in terms of

$$h(r_{ij}) \equiv f^c(r_{ij})^2 - 1\,. \tag{38}$$

Notice that for scalar correlation operator of Eq. (20) to respect the cluster properties one can impose

$$f^c(r \geq d^c) = 1\,. \tag{39}$$

The variational parameter d^c, to be fully explained later on, is the *central healing distance* encompassing the fact that when two-particles are further apart than d_c they are not anymore correlated. Hence, the quantity $h(r_{ij})$ can be seen as a smallness parameter for the cluster expansion, as it is indeed in the case of the "power-series" (PS) expansion scheme.

5.1 Two-body distribution function

In the calculation of the ground-state expectation value of any two-body scalar operator, it is very useful to employ the scalar two-body distribution function, $g^c(\mathbf{r}_1, \mathbf{r}_2)$, defined as

$$g^c(\mathbf{r}_1, \mathbf{r}_2) = \frac{A(A-1)}{\rho^2} \frac{\mathrm{Tr}_{12} \int dx_{3,\ldots,A} \Phi_0^*(X) \hat{\mathcal{F}}^\dagger \hat{\mathcal{F}} \Phi_0(X)}{\int dx_{1,\ldots,A}\ \Phi_0^*(X) \hat{\mathcal{F}}^\dagger \hat{\mathcal{F}} \Phi_0(X)}\,. \tag{40}$$

In terms of $g^c(\mathbf{r}_1, \mathbf{r}_2)$, the expectation value of a central the two-body potential reads

$$\langle v \rangle \equiv \sum_{i<j} (0|v_{ij}|0) = \frac{A(A-1)}{2} (0|v_{12}|0) = \frac{\rho^2}{2} \int d\mathbf{r}_{1,2}\, g^c(\mathbf{r}_1, \mathbf{r}_2) v(r_{12})\,. \tag{41}$$

For the first equality we have exploited the symmetry property of the wave function, which is due to the fact that $\mathcal{F}$ is symmetric and Φ_0 antisymmetric in the generalized particle coordinates. Since nuclear matter is uniform, $g^c(\mathbf{r}_1, \mathbf{r}_2) = g(r_{12})$, implying that $\langle v \rangle$ diverges with the number of particles. However, the potential energy per particle is finite and reads

$$\frac{\langle v \rangle}{A} = \frac{\rho}{2} \int dr_{12} g^c(r_{12}) v(r_{12})\,. \tag{42}$$

Particles 1 and 2 are denoted as *interacting particles* and are distinguished from the other particles in the medium.

The scalar two-body distribution function obeys the following sum rule

$$\rho \int d\mathbf{r}_{12}[g^c(r_{12}) - 1] = -1\,, \tag{43}$$

that can be easily derived by integrating Eq. (40) and using translation invariance of $g^c(r_{12})$. Note that the latter results is a consequence of the fact that the scalar two-body distribution function can interpreted as the joint probability of finding two particles with coordinates $\mathbf{r}_1$ and $\mathbf{r}_2$.

Following [39], in the following subsections we will provide a detailed description of the FR cluster expansion of the scalar two-body distribution function.

5.2 Cluster decomposition of $\hat{\mathcal{F}}^\dagger\hat{\mathcal{F}}$

In the purely central Jastrow case, the product of the correlation operator reduces to

$$\hat{\mathcal{F}}^\dagger\hat{\mathcal{F}} = \prod_{i<j} f^2(r_{ij}) = \prod_{i<j}[1 + h(r_{ij})]\,. \tag{44}$$

It is convenient to put aside the correlation between the interacting particles, denoted as "active correlation", while the others are called "passive correlations". Without loss of generality we can write

$$\begin{aligned}\hat{\mathcal{F}}^\dagger\hat{\mathcal{F}} &= f^2(r_{12}) \prod_{i<j\neq 1,2} [1 + h(r_{ij})] \\ &= f^2(r_{12})\Big(1 + \sum_{i\neq 1,2} X^{(3)}(\mathbf{r}_1, \mathbf{r}_2; \mathbf{r}_i) + \sum_{i<j\neq 1,2} X^{(4)}(\mathbf{r}_1, \mathbf{r}_2; \mathbf{r}_i, \mathbf{r}_j) + \dots\Big)\,.\end{aligned} \tag{45}$$

The generic cluster term $f^2(r_{12})X^{(n)}(\mathbf{r}_i, \dots, \mathbf{r}_n)$ correlates the positions of the two interacting particles and of the $n-2$ medium particles and should be considered as an n-body operator. For the sake of clarity we give the explicit expression of the first cluster terms

$$\begin{aligned}X^{(3)}(\mathbf{r}_1, \mathbf{r}_2; \mathbf{r}_i) &= h(r_{1i}) + h(r_{2i}) + h(r_{1i})h(r_{2i}) \\ X^{(4)}(\mathbf{r}_1, \mathbf{r}_2; \mathbf{r}_i, \mathbf{r}_j) &= h(r_{ij}) + h(r_{1i})h(r_{2j}) + h(r_{1i})h(r_{1j}) + h(r_{2i})h(r_{2j}) + h(r_{1i})h(r_{ij}) \\ &\quad + h(r_{2i})h(r_{ij}) + h(r_{1i})h(r_{2j})h(r_{ij}) + \dots\end{aligned} \tag{46}$$

5.3 Expansion of the numerator in cluster diagrams

The cluster expansion of the numerator can be performed by substituting the rhs of Eq. (45) in Eq. (40)

$$\text{num} = \frac{A(A-1)}{\rho^2}\text{Tr}_{12} \int dx_{3,\dots,A} f^2(r_{12})\Big(1 + \sum_{i\neq 1,2} X^{(3)}(\mathbf{r}_1, \mathbf{r}_2; \mathbf{r}_i) + \dots\Big)|\Phi_0(X)|^2\,. \tag{47}$$

The integration of the cluster terms on the squared modulus of the Fermi-gas wave function, which is invariant under the exchange of any particles, gives rise to a combinatory factor:

$$\sum_{i<j<,\cdots\neq 1,2}\int dx_{3,\ldots,A}X^{(N)}(\mathbf{r}_1,\mathbf{r}_2;\mathbf{r}_i,\mathbf{r}_j,\ldots)|\Phi_0(X)|^2$$
$$=\frac{(A-2)!}{(A-N)!(N-2)!}\int dx_{3,\ldots,A}X^{(N)}(\mathbf{r}_1,\mathbf{r}_2;\mathbf{r}_3,\ldots,\mathbf{r}_N)|\Phi^0(X)|^2\,. \tag{48}$$

Using the above result in Eq. (47) leads to

$$\text{num}=f^2(r_{12})\Big[\sum_{N=2}^{A}\frac{\rho^{N-2}}{(N-2)!}\int d\mathbf{r}_{3,\ldots,N}X^{(N)}(\mathbf{r}_1,\mathbf{r}_2;\mathbf{r}_3,\ldots,\mathbf{r}_N)g_N^{MF}(\mathbf{r}_1,\ldots,\mathbf{r}_N)\Big]\,, \tag{49}$$

where $X^{(2)}$=1 and we have introduced the mean-field N-body correlation function:

$$g_N^{MF}(\mathbf{r}_1,\ldots,\mathbf{r}_N)=\frac{A!}{(A-N)!}\frac{1}{\rho^N}\,\mathrm{Tr}_{1,\ldots,N}\int dx_{N+1,\ldots,A}|\Phi_0(X)|^2\,. \tag{50}$$

We now proceed by integrating out the variables $x_{N+1},\ldots,x_A$ from g_N^{MF} by using the orthogonality of single particle states.

$$g_N^{MF}(\mathbf{r}_1,\ldots,\mathbf{r}_N)=\frac{1}{\rho^N}\sum_{n_1<\cdots<n_N}\mathrm{Tr}_{1,\ldots,N}\Big[\mathcal{A}[\phi^\dagger_{n_1}(x_1)\ldots\phi^\dagger_{n_N}(x_N)]\mathcal{A}[\phi_{n_1}(x_1)\ldots\phi_{n_N}(x_N)]\Big]$$
$$=\frac{1}{\rho^N}\sum_{n_1,\ldots,n_N}\mathrm{Tr}_{1,\ldots,N}\Big[\phi^\dagger_{n_1}(x_1)\ldots\phi^\dagger_{n_N}(x_N)\mathcal{A}[\phi_{n_1}(x_1)\ldots\phi_{n_N}(x_N)]\Big]\,, \tag{51}$$

implying that if the number of particles, N, is larger than the number of quantum states, A, the mean-field N-body distribution function vanishes, i. e.

$$g_N^{cMF}(\mathbf{r}_1,\ldots,\mathbf{r}_N)=0\qquad\text{if}\qquad N>A\,. \tag{52}$$

We preliminary remark that this property is crucial for the exact cancellation of the unlinked diagrams of the numerator with the denominator to take place.

The antisymmetrization operator $\mathcal{A}$ can be written in the form

$$\mathcal{A}=1-\sum_{i<j}\hat{P}_{ij}+\sum_{i<j<k}(\hat{P}_{ij}\hat{P}_{jk}+\hat{P}_{ik}\hat{P}_{kj})+\ldots\,. \tag{53}$$

For a uniform system like nuclear matter the single particle states are normalized plane waves, see Eq. (14). Thus, the two-particle exchange operator, defined by the relation

$$\hat{P}_{ij}\phi_{n_i}(x_i)\phi_{n_j}(x_j)=\phi_{n_i}(x_j)\phi_{n_j}(x_i)\;. \tag{54}$$

can be written as

$$\hat{P}_{ij} = \hat{P}^{\sigma\tau}_{ij} \times P^{\mathbf{r}}_{ij}\,, \tag{55}$$

where

$$\hat{P}^{\sigma\tau}_{ij} = \frac{1}{4}(1+\sigma_{ij})(1+\tau_{ij}) \equiv \sum_{p=1}^{4} \Delta^p \hat{O}^p_{ij} \tag{56}$$

acts on the spin-isospin degrees of freedom of the nucleons' wave function, while

$$P^{\mathbf{r}}_{ij} = \exp[-i(\mathbf{k}_i - \mathbf{k}_j)\cdot \mathbf{r}_{ij}] \tag{57}$$

exchanges the radial coordinates of particles i and j.

Because Pauli matrices are traceless, in the purely Jastrow case, when the traces of Eq. (51) are carried out, the exchange operator reduces to its central part

$$\hat{P}_{ij} \to \frac{1}{\nu}\exp[-i(\mathbf{k}_i - \mathbf{k}_j)\cdot \mathbf{r}_{ij}]\,. \tag{58}$$

and one is left with

$$g^{MF}_N(\mathbf{r}_1,\ldots,\mathbf{r}_N) = \left(\frac{\nu}{\rho}\right)^N \sum_{k_1,\ldots,k_N} \phi^*_{\mathbf{k}_1}(\mathbf{r}_1)\ldots\phi^*_{\mathbf{k}_N}(\mathbf{r}_N)\mathcal{A}[\phi_{\mathbf{k}_1}(\mathbf{r}_1)\ldots\phi_{\mathbf{r}_N}(\mathbf{k}_N)]\Big]\,. \tag{59}$$

Therefore, g^{MF}_N can be written in terms of the Slater function, defined by

$$\ell(r_{ij}) = \frac{\nu}{\rho}\sum_{|\mathbf{k}|<k_F} \phi^*_{\mathbf{k}}(\mathbf{r}_i)\phi_{\mathbf{k}}(\mathbf{r}_j)\,. \tag{60}$$

In the limit of infinite volume, the sum over the discrete momenta can be replaced by an integral and it can be shown that

$$\ell(r_{ij}) = 3\Big[\frac{\sin(k_F r_{ij}) - k_F r_{ij}\cos(k_F r_{ij})}{(k_F r_{ij})^3}\Big]\,. \tag{61}$$

The first terms of the mean-field N-body distribution function reads

$$g^{MF}_n(\mathbf{r}_1,\ldots,\mathbf{r}_n) = 1 - \sum_{i<j}\frac{1}{\nu}\ell^2(r_{ij}) + \sum_{i<j<k}\frac{2}{\nu^2}\ell(r_{ij})\ell(r_{jk})\ell(r_{ki}) - \ldots\,. \tag{62}$$

The factors $1/\nu$ come from the normalization of the exchange operator of Eq. (58). In particular, producing a two-particle loop, $\ell^2(r_{ij})$, requires one exchange operator $\hat{P}_{ij}$ with the associated factor $1/\nu$. For a loop involving $n > 2$ particles and n-1 exchange operators, the corresponding factor is $(1/\nu)^{n-1}$. Moreover, there are two possible orderings of the exchange operators producing loops having more than two particles exchanged, bringing and additional factor 2.

We are now ready to give the general structure of the cluster decomposition for the numerator of Eq. (49). It is very useful to do this pictorially, introducing the so called "cluster diagrams". The diagrammatic rules are the following:

- The diagrams consist of dots (vertices) connected by different kinds of correlation lines. Open dots represent the active (or interacting) particles (1 and 2), while black dots are associated with passive particles, i.e. those in the medium. Integration over the coordinates of a passive particle leads to the appearance of a factor ρ.
- The dashed lines, representing the correlations $h(\mathbf{r}_{ij})$ and denoted as "correlation lines", cannot be superimposed.
- The statistical factor $-\ell(r_{ij})/\nu$, coming from the expansion of $g_n^{MF}(\mathbf{r}_1,\ldots,\mathbf{r}_n)$ is represented by an oriented solid "exchange line". The exchange lines must form closed loops and, as can be readily seen from the expansion of $\mathcal{A}$ in terms of the exchange operators of Eq. (53), different loops cannot have common points. Hence, the total exchange pattern consists in one or more non touching exchange loops.
- Each solid point must be reached by at least one correlation line; in fact in Eq. (49) each integration over $\mathbf{r}_i$ is associated with a term $X^{(N)}(\mathbf{r}_1,\mathbf{r}_2;\mathbf{r}_3,\ldots,\mathbf{r}_i,\ldots,\mathbf{r}_N)$.

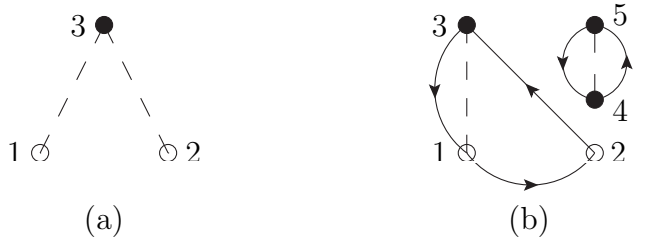

Figure 4: Examples of cluster diagrams.

Fig. 4 shows two examples of cluster diagrams whose analytic expressions read

$$(4.a) = \rho \int d\mathbf{r}_3 h(r_{13}) h(r_{23})\,, \tag{63}$$

$$(4.b) = -2\nu\Big(\frac{-\ell(r_{12})}{\nu}\Big) h(r_{12})\rho^3 \times \int d\mathbf{r}_3 d\mathbf{r}_4 d\mathbf{r}_5 \Big(-\frac{\ell(r_{23})}{\nu}\Big)\Big(-\frac{\ell(r_{13})}{\nu}\Big)\Big(-\frac{\ell^2(r_{45})}{\nu}\Big) h(r_{13}) h(r_{45}) \tag{64}$$

In Fig. 5 two examples of forbidden diagrams have been drawn. Diagram (5.a) is not allowed because the solid point 3 is not reached by any correlation line (moreover, between

Figure 5: Examples of not-allowed cluster diagrams.

points 2 and 4 there are two superimposed dashed lines); on the other hand in diagram(5.b) there are two touching exchange loops.

The cluster terms have no specific prefactor, except those coming from the exchange rules and a ρ factor for each integration. One might wonder where the $1/(n-2)!$ of Eq. (49) ended up. The factor is due to the counting of the permutations of the $n-2$ internal points and it is automatically taken into account by considering only topologically different graphs, or, in other words, by the fact that the labels of the solid points in the cluster diagrams are dummy indices. The only remnant of that factor is the inverse of what is usually called "symmetry factor", s. This counts the permutations of the solid points' labels that, without renaming the integration variables, leave the cluster term unchanged. For instance diagrams (a) and (b) of Fig. 6, being topologically identical, give the same contributions

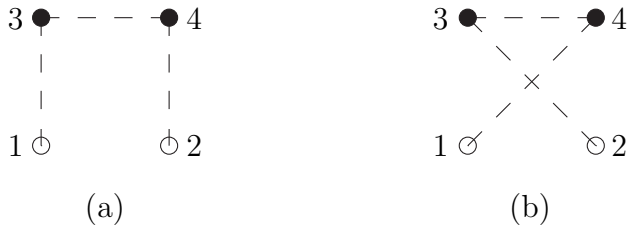

Figure 6: Topologically identical clusters diagrams.

$$(6.a) = \rho^2 \int d\mathbf{r}_3 d\mathbf{r}_4 h(r_{13}) h(r_{34}) h(r_{24})\,, \tag{65}$$

$$(6.b) = \rho^2 \int d\mathbf{r}_3 d\mathbf{r}_4 h(r_{14}) h(r_{34}) h(r_{23})\,. \tag{66}$$

As a consequence we take into account only one of them and no prefactors appear. On the other hand a prefactor $s = 1/2$ is associated with the diagram (a) of Fig. (7), because the exchange of points 3 and 4 leads to an identical expression, even without relabelling the dummy variables

$$(7.a) = \frac{\rho^2}{2} \int d\mathbf{r}_3 d\mathbf{r}_4 h(r_{13}) h(r_{14}) h(r_{34}) h(r_{23}) h(r_{24}) \,. \tag{67}$$

The reason of this fact lies in the constraint $i < j$ in the expansion of $\mathcal{F}^\dagger \mathcal{F}$ of Eq. (44), implying that a diagram analogous to diagram (7.a) with the points 3 and 4 exchanged does not appear in the cluster expansion.

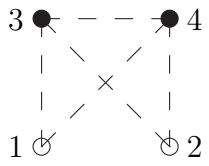

(a)

Figure 7: Graph with a prefactor $s = 1/2$ associated with.

Cluster diagrams may be *reducible* or *irreducible*. The integrals corresponding to irreducible diagrams cannot be factorized. Obviously an irreducible diagram must be *linked*, i.e. each couple of points must be connected by a sequence of lines, which can be both correlation and exchange lines. For instance, diagrams (4.a), (6.a), (6.b), (7.a) are linked and irreducible, while diagram (4.b) is unlinked (and reducible). If we add to the irreducible diagram (4.a) the correlation line $h(\mathbf{r}_{34})$, we obtain the reducible diagram of Fig. (8), the expression of which reads

$$(8.a) = \rho^2 \int d\mathbf{r}_3 d\mathbf{r}_4 h(r_{13}) h(r_{23}) h(r_{34}) \,, \tag{68}$$

$$= \rho \int d\mathbf{r}_3 h(r_{13}) h(r_{23}) \times \rho \int d\mathbf{r}_{34} h(r_{34}) \,, \tag{69}$$

which is just the cluster term of (4.a) multiplied by the cluster term of the added part.

Translational invariance gives rise to a factor V for each unlinked part of the diagram but for the one containing the external points 1 and 2. Therefore, the order of magnitude of a cluster diagram is $V^{N_u - 1}$, where N_u is the number of unlinked parts. For example, the order of magnitude of the linked diagram (4.a) is 1 while the one of diagram (4.b), having two unconnected parts, is V.

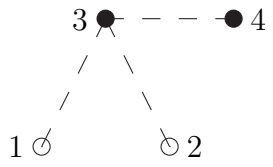

(a)

Figure 8: Linked and reducible diagram.

5.4 Expansion of the denominator in cluster diagrams.

The same procedure followed for the expansion of the numerator can be used for the denominator. However, in this case there are no interacting particles; hence $\hat{\mathcal{F}}^\dagger\mathcal{F}$ can be conveniently expanded as

$$\hat{\mathcal{F}}^\dagger\hat{\mathcal{F}} = \left(1 + \sum_{i<j} X^{(2)}(\mathbf{r}_i, \mathbf{r}_j) + \sum_{i<j<k} X^{(3)}(\mathbf{r}_i, \mathbf{r}_j, \mathbf{r}_k) + \dots\right) \tag{70}$$

where the cluster term $X^{(N)}$ correlates N particles. The explicit expressions for $N = 2$ and $N = 3$ are

$$\begin{aligned} X^{(2)}(\mathbf{r}_i, \mathbf{r}_j) &= h(r_{ij})\,, \\ X^{(3)}(\mathbf{r}_i, \mathbf{r}_j, \mathbf{r}_k) &= h(r_{ij})h(r_{ik}) + h(r_{ik})h(r_{jk}) + h(r_{ij})h(r_{jk}) + h(r_{ij})h(r_{jk})h(r_{ik})\,. \end{aligned} \tag{71}$$

Substituting the expansion of $\hat{\mathcal{F}}^\dagger\mathcal{F}$ of Eq. (70) in the denominator of Eq. (40) and exploiting the invariance of $|\Psi^0_{MF}|^2$ under any two-particle exchange, one finds

$$\text{den} = 1 + \sum_{N=2}^{A} \frac{\rho^N}{N!} \int d\mathbf{r}_1 \dots d\mathbf{r}_N g_N^{MF}(\mathbf{r}_1, \dots, \mathbf{r}_N) X^{(N)}(\mathbf{r}_1, \dots, \mathbf{r}_N)\,, \tag{72}$$

with g_N^{MF} defined in Eq. (50).

Comparing Eqs. (49) and (72), it can easily realized that the diagrammatic rules for the denominator are very similar to those of the numerator. The only difference is that the cluster diagrams of the denominator only have solid points, hence their order of magnitude is V^{N_u}. In Fig. 9 two examples of cluster diagrams coming from the expansion of the denominator are depicted.

5.4.1 Two-body distribution function as a sum of cluster diagrams.

The ratio of Eq. (40) involves two infinite series of cluster terms, corresponding to the expansion of the numerator and of the denominator.

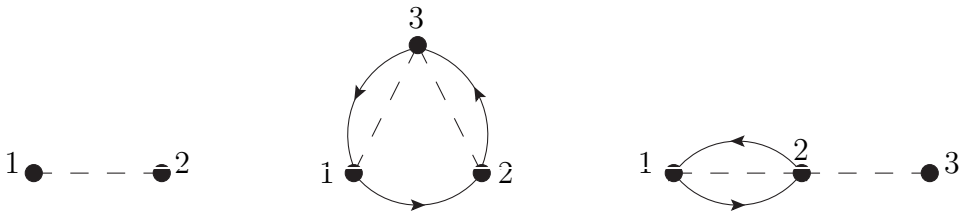

Figure 9: Examples of cluster diagrams of the denominator.

Let us consider a generic n body linked (reducible or irreducible) cluster diagram, $\mathcal{L}_n$, of the numerator [63], where each internal point is connected to the points 1 and 2 by at least one continuous path of correlation and/or exchange lines. Each cluster diagram of the numerator can be built as a product of $\mathcal{L}_n$ times a factor $\mathcal{U}_q$, with $q = A - n$, representing the sum of all the q body unlinked diagrams

$$\text{num} = \sum_{n=2}^{A} \mathcal{L}_n \times \mathcal{U}_{A-n} \,. \tag{73}$$

An example of the above equation is displayed in Fig. 10, where the diagram (4.a) belongs to $\mathcal{L}_3$ and the sum of the diagrams enclosed in round parenthesis is $\mathcal{U}_{A-3}$. Considering the

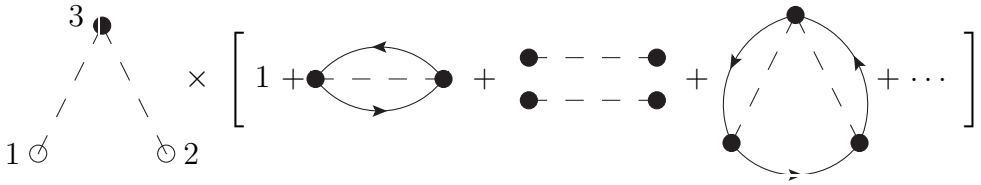

Figure 10: Series of unlinked diagrams associated with $L_n = (4.a)$.

expression of the expansion of the denominator, it is readily seen that

$$\text{den} = \sum_{n=1}^{A} \mathcal{U}_n \,. \tag{74}$$

Hence, one might naively think that the denominator cancels the disconnected diagrams of the numerator in the thermodynamic limit, $A \to \infty$, only. However, by using the property

of Eq. (52) it is possible to extend up to infinity the upper limits of all the sums appearing in Eqs. (49) and (72), yielding

$$\begin{aligned} \text{num} &= \sum_{n=2}^{\infty} \mathcal{L}_n \times \sum_{q=1}^{\infty} \mathcal{U}_q \\ \text{den} &= \sum_{n=1}^{\infty} \mathcal{U}_n \,, \end{aligned} \tag{75}$$

that proves the fundamental *linked cluster property*

$$g_2^c(r_{12}) = \sum_{n=2}^{\infty} \mathcal{L}_n \,. \tag{76}$$

Because of this property, which is a common feature of diagrammatic expansion techniques, the divergent terms of the numerator and of the denominator cancel out, giving rise to finite physical quantities. It has to be remarked that for Fermi systems the exact cancellation of unlinked diagrams still holds when spin-isospin dependent correlation are considered.

5.5 Perturbative schemes

In this subsection we briefly present two possible choices for the smallness parameter of the cluster expansion, namely, the expansion in the number of points and the power series (PS) expansion.

Expansion in the number of points Within this scheme, the order of magnitude of a linked diagram is given by the number of its internal points: expanding the two body distribution function at $n = m$. As a factor ρ^{n-2} is associated with n internal points, the smallness parameter is nothing but the density.

This was the first scheme adopted for classifying diagrams of Fermi liquids; however the series is rapidly convergent for low-density regimes only. This is not the case for nuclear matter, as found by the authors of Ref. [64]. They have shown that at the equilibrium density, the 1-5 body cluster contributions to the energy of SNM are 22.1 MeV, 43.7 MeV, 10.8 MeV, 3.4 MeV, and 2.6 MeV, while those with $n > 5$ give 0.8 MeV. The computational cost of this approach exponentially increases with the number of internal points: actual calculations do not go beyond the three-body cluster contribution in the case of spin-isospin dependent operators.

It has to be noted that the expectation value of the Hamiltonian at any finite order of the expansion in the number of internal points is unbound. The main reason for this lies in the normalization of the wave function that is not properly taken into account. Nevertheless, as it will be fully explained at a later stage, a procedure usually employed to obtain the correlation function $f^p(r)$ consists in minimizing the two-body cluster contribution to the energy per

particle imposing constraints on the variational parameters of the correlation functions.

Power series (PS) expansion Suppose to multiply each correlation line $h(r_{ij})$ by a parameter α, it follows that the term of order m in the PS expansion scheme [58] of $g_2(r_{12})$, denoted as $g_2^{\alpha_n}$, corresponds to the terms of order α^m resulting from the sum of Eq. (76). Of course the zeroth order corresponds to the mean field results, $g_2^{\alpha_0} = g_2^{MF}$.

A given order of the power series expansion mixes different orders of the expansion in the number of points. For instance the first order in PS includes all of the 2-body diagrams, ten 3-body diagrams and nine 4-body diagrams.

A remarkable feature of the PS scheme is that the sum rule of Eq. (43) for the two-body distribution function is satisfied at any order. A very simple argument to proof this statement, that can be found in [39], is the following. For any choice of α the sum rule reads

$$\rho \int d\mathbf{r}_{12} (\sum_n \alpha^n g_2^{c\,\alpha_n}(r_{12}) - 1) = -1\,. \tag{77}$$

Since the mean-field two-body distribution function satisfies the former sum rule, it turns out that

$$\rho \int d\mathbf{r}_{12} \sum_{n>1} \alpha^n g_2^{c\,\alpha_n}(r_{12}) = 0\,. \tag{78}$$

The integral of the series is zero for any choice of α within the convergence radius, thus the integral of each of the coefficients $g_2^{c\,\alpha_n}$ has to be zero.

The drawback of the PS expansion is that it does not appropriately describe the short-range behavior of the pair function, which is crucial for the calculation of the binding energy. The factor $f(r_{12})$, while being set aside in Eq. (45), does not in fact multiply all terms of the expansion.

5.6 Fermi Hyper-Netted Chain (FHNC) and RFHNC schemes

To allow for a good description of both the short and the long range behavior of the pair function, the development of a scheme in which infinite sets of cluster diagrams are summed up is required. This goal is achieved by the FHNC summation procedure, two versions of which had been originally proposed: one by Fantoni and Rosati [58, 65, 59] and the other by Krotscheck and Ristig [66, 60].

The two schemes are essentially complementary: the one by Krotscheck and Ristig is better suited to the treatment of long-range correlations, while the FR is more convenient for the evaluation of the energy in the presence of strong short-range correlations. Since in this work have been dealing with the calculation of the expectation value of the potential, we have extensively used the FR approach, that we present for the case of a Fermi liquid and a wave function with Jastrow-type correlations (for which FHNC has been originally developed).

In what follows, we will not assume that the reducible clusters diagrams cancel out, which is strictly true only for a uniform Fermi liquid described by scalar correlations, as rigorously proved in Ref. [58]. In Section 6.4 we will show how the cancellation mechanism works in the case of the 3-body cluster contributions.

The first detailed classification of the cluster diagrams, limited to the bosonic case, can be found in the fundamental work of J.M.J. van Leeuwen, J. Groeneveld and J. de Boer [67], while the extension to Fermi systems is extensively analyzed in the more recent Refs. [39, 63].

5.6.1 Vertex Corrected Irreducible (VIC) diagrams

In this subsection we will show that, when scalar correlations only are considered, reducible diagrams can be included in the calculation of the two-body scalar distribution function through vertex corrections to the irreducible diagrams.

For the sake of introducing the reducible diagrams, the correlation line $h(\mathbf{r}_{34})$ had been attached to the point 3 of diagram (4.a). It is readily seen that to the point 3 we can add all the possible linked one-body diagrams, or, in other words, all the linked diagrams contributing to the one-body correlation function $g(\mathbf{r}_3)$. The net result is that the sum of all the reducible diagrams having diagram (4.a) as the irreducible part, can be represented by diagram (4.a) with the vertex 3 *renormalized*, in the sense that it is vertex corrected by ξ_d, which in the case of translation invariant system is a constant

$$\xi_d = 1 + \sum(\text{linked one-body cluster terms}) = g^c(\mathbf{r})\,. \tag{79}$$

A pictorial representation of $g^c(\mathbf{r})$ is given in Figure (11).

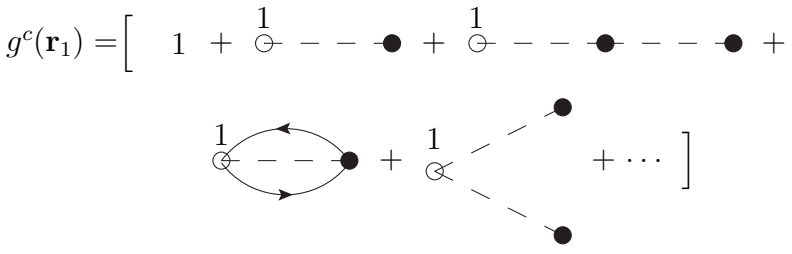

Figure 11: Diagrams contributing to $g^c(\mathbf{r}_1)$, i.e. to the vertex correction ξ_d. The same diagrams but the first of the second line contribute to ξ_e as well.

Note that there are no restrictions on the kind of cluster terms in the sum, because in diagram (4.a) no exchange lines reach the point 3, which is dubbed "d" point (the label d comes from "dynamical correlations" which is the name originally given to the correlation

lines). Conversely, if the reducibility point is reached by exchange lines, like, for example, the point 3 of diagram (4.b), which is an "e" point, then, to avoid the forbidden superposition of exchange lines, the cluster diagrams of the vertex correction needs to be attached to point 3 through a correlation line. It follows that there are two kinds of vertex corrections: ξ_d and ξ_e, for reducibility points of type d and e, respectively.

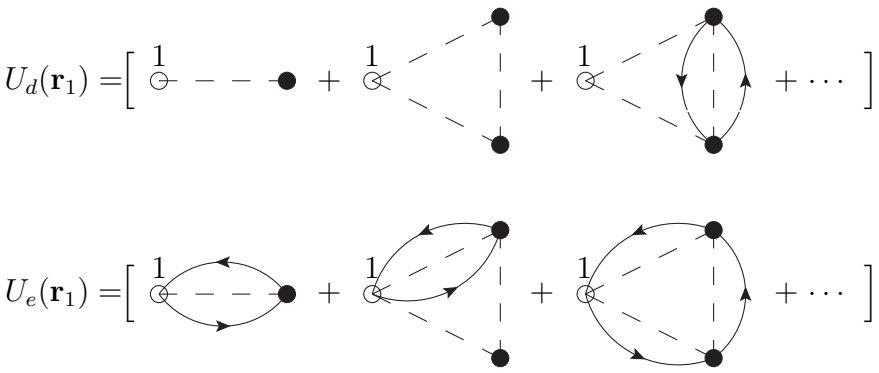

Figure 12: Diagrams belonging to $U_d(\mathbf{r}_1)$ and to $U_e(\mathbf{r}_1)$.

Actually there is a third type of vertex correction, occurring when the reducibility point is an internal point connected to the rest of the diagram containing the external points only through exchange lines. This correction cannot be the full ξ_e, since any solid point must be reached by at least one correlation line, hence in this case the vertex correction is $\xi_c = \xi_e - 1$.

The above procedure can be applied to the external point of diagram (4.a) and to all irreducible diagrams. The conclusion is that the sum of reducible and irreducible diagrams may be seen as a sum of vertex corrected irreducible diagrams, which are called "VIC diagrams", namely irreducible diagrams whose points carry the vertex corrections ξ_d, ξ_e and ξ_c. Note that, taking into account vertex corrections, diagram (5.a), without the two superimposed $h(\mathbf{r}_{34})$ lines, is allowed, because point 3 is vertex corrected by ξ_c. Consequently, the second diagrammatic rule does not hold for VIC diagrams that may have internal points reached by exchange lines only.

For a uniform system like nuclear matter, the one body distribution function is equal to unity, $g_1(\mathbf{r}) = 1$. This implies the sum rule $\xi_d = 1$ that is an useful check for the accuracy of the vertex corrections calculation.

We define a new set of one-body VIC diagrams $U_d(\mathbf{r}_1)$ and $U_e(\mathbf{r}_1)$ in terms of the following

equations

$$\xi_d = [1 + U_e(\mathbf{r}_1)] \exp[U_d(\mathbf{r}_1)] \tag{80}$$

$$\xi_e = \exp[U_d(\mathbf{r}_1)] \,. \tag{81}$$

The external point 1 of the diagrams belonging to $U_d(\mathbf{r}_1)$ is not reached by any exchange lines; conversely in those forming $U_e(\mathbf{r}_1)$ the point 1 *must* be reached by a loop of exchange lines. Moreover diagrams in both $U_d(\mathbf{r}_1)$ and $U_e(\mathbf{r}_1)$ cannot be built by pieces connected only by means of the point 1. The exponential in the above equations is due to the fact that any number of d-structures forming U_d can be attached to the point 1. Since the symmetry factor for n topologically identical structures is $1/n!$, the global contribution of U_d is given by $\sum_n (1/n!) U_d(\mathbf{r}_1)^n$.

For the sake of illustration, some of the diagrams belonging to $U_d(\mathbf{r}_1)$ and to $U_e(\mathbf{r}_1)$ are depicted in Fig. 12.

5.6.2 Simple and composite diagrams

When in an irreducible diagram it is possible to distinguish two or more pieces that are connected with the rest of the diagram by means of the point i and j only, we denote these parts as *subdiagrams* [67]. Two or more subdiagrams are said to form *parallel connections* between the external points 1 and 2 when the whole diagram consists of two or more parts which are only connected by means of points 1 and 2. As no integration is carried out over the two external points, a factorization of the integral associated with the diagram takes place.

An irreducible diagram consisting of two or more parallel subdiagrams is called *composite* or $X - diagram$. When such division in parallel subdiagrams is not possible the diagram is called *simple*. For example diagram (4.a) is simple, as well as those of Figs. 6 and 7. Ignoring the unlinked part, diagram (4.b) is composite, as shown in Fig. 13.

As for the vertex corrections, composite diagrams can be classified on the base of the kind of their external points 1 and 2. The set of composite diagrams with only correlation line reaching points 1 and 2, like diagram (a) of Fig. 14, are denoted with X_{dd}. When two exchange lines are attached to point 1 (2) the corresponding composite diagrams are labelled with X_{ed}

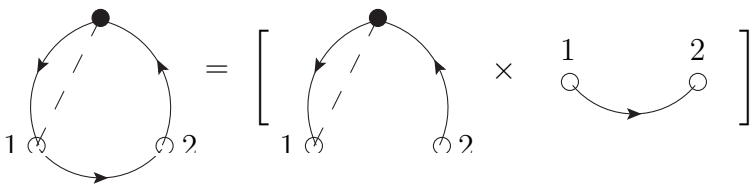

Figure 13: A composite diagram decomposed in simple subdiagrams.

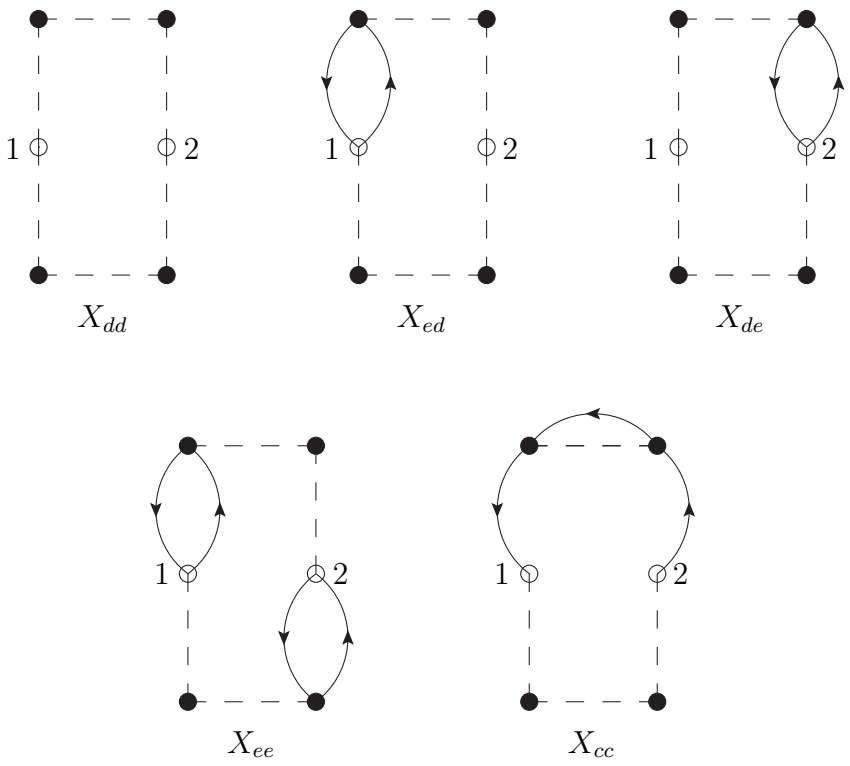

Figure 14: Classification of composite diagrams based on the kind of the external points.

(X_{de}), see diagrams (b) and (c) of Fig. 14. Analogously, diagram (14.d) belongs to the set X_{ee} since two statistical lines arrive at both external points. To build the *ee* diagrams with the external points in the same statistical loop, it is convenient to define composite diagrams where a statistical open loop starts from the external point 1 and ends to the external point 2, like for instance diagram (e) of Fig. 14 and the one in Fig. 13. Note that the set of these diagrams, denoted by X_{cc}, does not directly contribute scalar two-body distribution function.

5.6.3 Nodal diagrams

An important concept concerning the diagrams classification is the possible occurrence of a "node". Such a node is an internal point through which all possible paths joining the external points 1 and 2 pass through. A diagram with one ore more nodes is denoted as "nodal" diagram. Diagrams (4.a), (6.a) and (6.b) are nodal.

A nodal diagram is also necessarily a simple diagram, but not all simple diagrams are nodal,

as for example diagram (7). Non nodal simple diagrams are called "elementary" diagrams, or $E-diagrams$. Nodal diagrams can be classified according to the same scheme, based on the kind of external points, adopted for composite diagrams. Examples of diagrams belonging to sets N_{dd}, N_{ed}, N_{de}, N_{ee} and N_{ee} are depicted in Fig. 15.

5.7 FHNC equations

Consider a nodal diagram contributing to $N_{xy}(r_{12})$ and label 3 the node closest to point 1. All the nodal diagrams can then be found by convoluting the sum of all non-nodal $1-3$ subdiagrams, $X_{xx'}(r_{13})$, with the set of $3-2$ subdiagrams $X_{y'y}(r_{23})+N_{y'y}(r_{23})$ (with or without nodes). This leads to the following integral equation

$$N_{xy}(r_{12}) = \sum_{x'y'} \rho \int d\mathbf{r}_3 X_{xx'}(r_{13}) \zeta_{x'y'} [X_{y'y}(r_{23}) + N_{y'y}(r_{23})] \,, \tag{82}$$

the indexes x and y running over the types d and e of the external point. The coefficients $\zeta_{x'y'}$, accounting for the vertex corrections and for the proper treatment of the exchange loops, read

$$\zeta_{dd} = \xi_d \quad , \quad \zeta_{de} = \zeta_{ed} = \xi_e \quad , \quad \zeta_{ee} = 0 \,. \tag{83}$$

In order to better understand the effect of the long-range part of the correlation function, it is worth rewriting the convolution Eq. (82) in momentum space

$$\tilde{N}(k) = \rho \xi \tilde{X}(k) [\tilde{X}(k) + \tilde{N}(k)] \,. \tag{84}$$

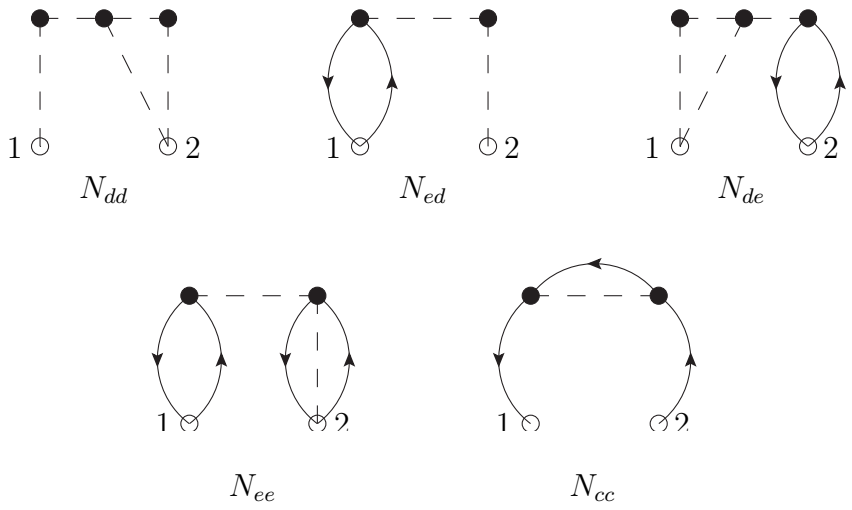

Figure 15: Classification of nodal diagrams according to the kind of the external points.

where $\tilde{N}(k)$ and $\tilde{X}(k)$ are the Fourier transforms of the nodal and composite functions, respectively. Note that we have omitted the subscripts referring to the kind of verices, whose presence is irrelevant to the purpose of this discussion. Solving Eq. (84) for $\tilde{N}(k)$ yields

$$\tilde{N}(k) = \frac{\rho\xi\tilde{X}(k)}{1-\rho\xi\tilde{X}(k)}\,. \tag{85}$$

As a further simplification, consider the nodal diagram $N^n(r)$ formed by n correlation lines $h(r)$. The analytic expression of $\tilde{N}^n(k)$ can be easily derived iterating Eq. (84), where $\tilde{X}(k)$ has to be replaced by its first order contribution $\tilde{h}(k)$

$$\tilde{N}^n(k) = (\rho\xi)^{n-1}\,\tilde{h}(k)^n\,. \tag{86}$$

Therefore, the sum of all the $N^n(r)$ is given by

$$\sum_n \tilde{N}^n(k) = \frac{\rho\xi\tilde{h}(k)}{1-\rho\xi\tilde{h}(k)}\,, \tag{87}$$

which is in turn a particular case of Eq. (85). If $h(r)$ is long ranged, say $h(r) \to \alpha/r^2$ for $r \to \infty$, then $\tilde{h}(k) \to -\alpha/(2\pi k)$ for $k \to 0$. Consequently, each $\tilde{N}^n(k)$ is more divergent than $\tilde{h}(k)$ in the long wavelength limit, while their sum is well behaved as it diverges like $\tilde{h}(k)$. From this fact, we can gather that the expansion in the number of points diverges at any finite order, while the chain summations leads to a well behaved long range limit.

The iterative equation for N_{cc}, cannot be written in a form analogous to that of Eq. (82). It differs more from those given in ref., where because the cyclic nodal diagrams do not show not all the cancellations occurring when the cancellation of reducible diagrams had been assumed from the very beginning [68]. We need to distinguish two different kinds of external points: the point x which is reached by an exchange line and at least one correlation line and the point p which is reached by an exchange line only. Hence four type of nodal cyclic functions, namely N_{cc}^{xx}, N_{cc}^{xp}, N_{cc}^{px} and N_{cc}^{pp} and correspondingly three type of composite functions, $X_{cc}^{\alpha\beta}$, have to be properly taken into account. For instance, the convolution of N_{cc}^{xx} with any other of the cyclic functions brings a vertex correction ξ_e, whereas the convolution of two pp cyclic functions requires a ξ_c vertex correction. The four nodal equations are given by

$$\begin{aligned}
N_{cc}^{xx}(r_{12}) &= \rho\int d\mathbf{r}_3\xi_e X_{cc}(r_{13})[X_{cc}(r_{32}) + N_{cc}^{xx}(r_{32}) + N_{cc}^{px}(r_{32})] \\
N_{cc}^{xp}(r_{12}) &= \rho\int d\mathbf{r}_3\xi_e X_{cc}(r_{13})\Big[-\frac{1}{\nu}\ell(r_{32}) + N_{cc}^{xp}(r_{32}) + N_{cc}^{pp}(r_{32})\Big] \\
N_{cc}^{px}(r_{12}) &= -\frac{\rho}{\nu}\int d\mathbf{r}_3\xi_e \ell(r_{13})[X_{cc}(r_{32}) + N_{cc}^{xx}(r_{32})] + \xi_c\ell(r_{13})N_{cc}^{px}(r_{32}) \\
N_{cc}^{pp}(r_{12}) &= -\frac{\rho}{\nu}\int d\mathbf{r}_3\xi_e \ell(r_{13})N_{cc}^{xp}(r_{32}) + \xi_c\ell(r_{13})\Big[N_{cc}^{pp}(r_{32}) - \frac{1}{\nu}\ell(r_{32})\Big]\,,
\end{aligned} \tag{88}$$

with

$$N_{cc}^{px}(r_{12}) = N_{cc}^{xp}(r_{12}) \ . \tag{89}$$

The total cyclic nodal functions is given by

$$N_{cc}(r_{12}) = N_{cc}^{xx}(r_{12}) + N_{cc}^{xp}(r_{12}) + N_{cc}^{px}(r_{12}) + N_{cc}^{pp}(r_{12}) \ . \tag{90}$$

Summing the Eqs. (88), one can solve the following integral equation for the total N_{cc}

$$\begin{aligned} N_{cc}(\vec{r}_{12}) = \rho \int_V d\mathbf{r}_3 X_{cc}(r_{13}) \xi_e \Big[X_{cc}(r_{32}) + N_{cc}(r_{32}) - \frac{\ell(\vec{r}_{32})}{\nu} \Big] \\ - \frac{\ell(r_{13})}{\nu} \xi_e \Big[X_{cc}(r_{32}) + \mathcal{P}(r_{32}) \Big] \\ - \frac{\ell(r_{13})}{\nu} \xi_c \Big[- \frac{\ell(r_{32})}{\nu} + N_{cc}(r_{32}) - \mathcal{P}(r_{32}) \Big] \ , \end{aligned} \tag{91}$$

where $\mathcal{P}$ is given by

$$\mathcal{P}(r_{12}) = \rho \int_V d\mathbf{r}_3 \xi_e X_{cc}(r_{13}) \Big[X_{cc}(r_{32}) + N_{cc}(r_{32}) - \frac{\ell(\vec{r}_{32})}{\nu} \Big] \ . \tag{92}$$

At this stage, it is worth introducing the expressions for the *partial* two-body scalar distribution functions

$$\begin{aligned} g_{dd}^c(r_{12}) &= f^2(r_{12}) \exp[N_{dd}(r_{12}) + E_{dd}(r_{12})] \ , \\ g_{de}^c(r_{12}) &= g_{ed}^c(r_{12}) = N_{de}(r_{12}) + X_{de}(r_{12}) \ , \\ g_{ee}^{c\,dir}(r_{12}) &= g_{dd}^c(r_{12}) \{ N_{ee}(r_{12}) + E_{ee}^{dir}(r_{12}) + [N_{de}(r_{12}) + E_{de}(r_{12})]^2 \} \ , \\ g_{ee}^{c\,exch}(r_{12}) &= -\nu \, g_{dd}^c(r_{12}) \Big[N_{cc}(r_{12}) - \frac{1}{d} \ell(r_{12}) + E_{cc}(r_{12}) \Big]^2 + E_{ee}^{exch}(r_{12}) g_{dd}^c(r_{12}) \ , \\ g_{cc}(r_{12}) &= N_{cc}(r_{12}) + X_{cc}(r_{12}) - \frac{1}{\nu} \ell(r_{12}) \ . \end{aligned} \tag{93}$$

where $E_{xy}(\vec{r}_{12})$ represent the sum of the xy elementary diagrams. The explanation for the presence of the exponential in the above equations is analogous to the one given for the vertex corrections of Eq. (81). Note that, as for the vertex corrections, there are no exponentials associated with the $e-$ structures, as two exchange loops cannot be superimposed.

The composite functions, which in turn can be seen as generalized links, are defined as

$$\begin{aligned} X_{dd}(r_{12}) &= g_{dd}^c(r_{12}) - N_{dd}(r_{12}) - 1 \\ X_{de}(r_{12}) &= X_{ed}(r_{12}) = g_{dd}^c(r_{12}) [N_{de}(r_{12}) + E_{de}(r_{12})] - N_{de}(r_{12}) \ , \\ X_{ee}(r_{12}) &= g_{dd}^c(r_{12}) \Big\{ N_{ee}(r_{12}) + E_{ee}(r_{12}) + [N_{de}(r_{12}) + E_{de}(r_{12})]^2 \\ &\quad - \nu \Big[N_{cc}(r_{12}) - \frac{1}{\nu} \ell(r_{12}) + E_{cc}(r_{12}) \Big]^2 \Big\} - N_{ee}(r_{12}) \\ X_{cc}(r_{12}) &= g_{dd}^c(r_{12}) [N_{cc}(r_{12}) - \frac{1}{\nu} \ell(r_{12}) + E_{cc}(r_{12})] - N_{cc}(r_{12}) + \frac{1}{\nu} \ell(r_{12}) \end{aligned} \tag{94}$$

The functions $U_{d,e}$ appearing in eq. (81) and entering the vertex corrections $\xi_{d,e}$ are solutions of the following integral equations

$$\begin{aligned} U_d = \rho \int_V d\mathbf{r}_{12} \xi_d [& X_{dd}(r_{12}) - E_{dd}(r_{12}) - S_{dd}(r_{12})(g_{dd}(r_{12}) - 1)] \\ & + \xi_e [X_{de}(r_{12}) - E_{de}(r_{12}) - S_{dd}(r_{12}) g_{de}(r_{12}) \\ & - S_{de}(r_{12})(g_{dd}(r_{12}) - 1)] + E_d \ , \end{aligned}$$

$$\begin{aligned} U_e = & \rho \int_V d\vec{r}_{12} \xi_d [X_{ed}(r_{12}) - E_{ed}(r_{12})] + \xi_e [X_{ee}(r_{12}) - E_{ee}(r_{12})] \\ & - \xi_d \left[S_{dd}(r_{12}) g_{ed}(r_{12}) + S_{ed}(r_{12})(g_{dd}(r_{12}) - 1) \right] - \xi_e [S_{ee}(r_{12})(g_{dd}(r_{12}) - 1) \\ & + S_{ed}(r_{12}) g_{de}(r_{12}) + S_{dd}(r_{12}) g_{ee}(r_{12}) + S_{de}(r_{12}) g_{ed}(r_{12}) - 2d S_{cc}(r_{12}) g_{cc}(r_{12})] \\ & - \ell(r_{12}) [\mathcal{N}^p_{cc}(r_{12}) - \frac{1}{\nu} \ell(r_{12})] + E_e \ , \end{aligned} \tag{95}$$

with

$$\begin{aligned} & S_{xy}(\vec{r}_{12}) = \frac{1}{2} N_{xy}(r_{12}) + E_{xy}(r_{12}) \ , \\ & \mathcal{N}^x_{cc}(r_{12}) = N^{xx}_{cc}(r_{12}) + N^{xp}_{cc}(r_{12}) = \xi_e \rho \int_V d\mathbf{r}_{32} X_{cc}(r_{13}) [X_{cc}(r_{32}) + N_{cc}(r_{32}) - \frac{1}{\nu} \ell(r_{32})] \ , \\ & \mathcal{N}^p_{cc}(r_{12}) = N^{pp}_{cc}(r_{12}) + N^{px}_{cc}(r_{12}) = N_{cc}(r_{12}) - \mathcal{N}^x_{cc}(r_{12}) \ , \end{aligned} \tag{96}$$

and E_d and E_e are the one–body elementary diagrams with external point d and e respectively.

The FHNC equations are solved numerically by means of iterative procedures. At the nth step, the nodal diagrams and the 1-body structures resulting from the step $n-1$, namely $N_{xy}(n-1)$ and $U_x(n-1)$, are employed to compute the partial scalar two-body distribution functions as well as the composite functions $X_{xy}(n)$. Hence, the new nodal functions and the 1-body structures are calculated making use of those quantities.

The iterative procedure is stopped when the difference between the values of a test quantity, e.g. the nodal diagrams or the energy, computed in two successive iterations is smaller than a given convergence parameter. In order for the procedure to start, the nodal diagrams are initially set to zero, while for vertex corrections one sets $\xi_d = \xi_e = 1$.

For dense systems, like liquid helium or nuclear matter, the convergence may be difficult to reach, and one may want to smooth out the iterative process. One of the most used technique consists in multiplying by a "mixing parameter", $0 < \alpha_{mix} < 1$, the nodal diagrams resulting from the step $n-1$ of the iteration procedure and by $1-\alpha_{mix}$ those obtained in the current step n. Then all the other quantities at the iteration n, like, for instance, the composite diagrams, are obtained using the mixture

$$\alpha_{mix} N_{xy}(n-1) + (1 - \alpha_{mix}) N_{xy}(n) \, . \tag{97}$$

In order to close the FHNC scheme, an iterative equation for the elementary diagrams would be required. However, because of their topological structure, a consistent treatment of the elementary diagrams based on two-body kernel equations, like those for the nodal and composite diagrams, is not feasible.

The simplest approximation consists in neglecting all the elementary diagrams, setting $E_{xy} = 0$ (FHNC/0 approximation). Although elementary diagrams are neglected in this approach, FHNC/0 provides a very good description of the long-range part of the two-body distribution function, and it is also accurate enough at short interparticle distances (although $E_{xy}(r)$ are short-range functions). For instance, in nuclear matter calculation the elementary diagrams' contribution is likely to be small, provided that accurate minimization procedures, like the one described in Section 6.5, are performed.

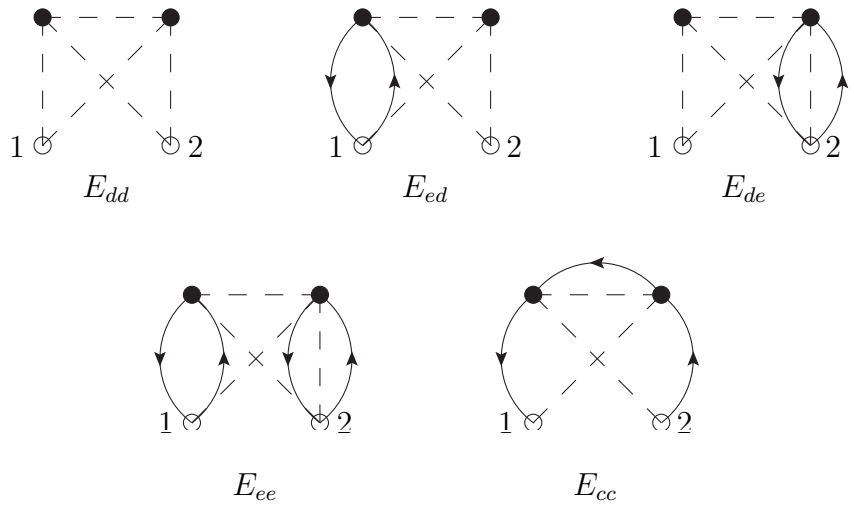

Figure 16: Some 4-body elementary diagrams.

A brute force approach based on the direct calculation of the $n-$body elementary diagrams E_n, like the $4-$body diagrams of Fig. 16, and the inclusion of their contributions in the FHNC equations, (FHNC/n approximation) does not seem to be a promising strategy. In fact, in the cases where the elementary diagrams give appreciable effects, like in liquid helium, the FHNC/n series shows poor convergence.

A more reliable procedure for bosonic systems, denote as *scaling approximation* (HNC/s) [33] amounts to approximating the full set of elementary diagram by αE_4. The scaling parameter, α, is determined by matching the expectation values of the kinetic energy obtained following the Pandharipande-Bethe and the Jackson-Feenberg prescriptions, prescriptions, to be discussed in the next Section, which in an exact calculation would give the same results. The existence of a scaling property for fermionic systems is not at all clear, as there are different

classes of elementary diagrams, depending on the kind of the external points. Nevertheless, the fermionic generalization of the scaling approximation has been used in liquid ^{3}He with some success [69].

Preliminary results obtained using iterative equations with four-body kernels are quite encouraging, as the difference with respect to Variational Monte Carlo results turns out to be much smaller with respect to the FHNC/0 case [70].

The total *scalar* two–body distribution function is given by the sum of the four different kinds of the partial two-body distribution functions, multiplied by the appropriate vertex corrections

$$g^c(r_{12}) = \xi_d^2 g^c_{dd}(r_{12}) + \xi_d \xi_e [g^c_{de}(r_{12}) + g^c_{ed}(r_{12})] + \xi_e^2 [g^{c\,dir}_{ee}(r_{12}) + g^{c\,exch}_{ee}(r_{12})] \,. \tag{98}$$

The numerical solution of the coupled FHNC integral equations is not trivial at all. Moreover,the numerical convergence of the solution does not ensure that this solution is acceptable from the physical point of view, as neglecting elementary diagrams could in principle lead to a violation of the variational principle. A useful tool to check both the numerical and the theoretical accuracy of the calculations is the fulfillment of the sum rule of the scalar distribution function of Eq. (43). Comparing the values of the kinetic energy expectation value obtained using the Pandharipande-Bethe and the Jackson-Feenberg prescriptions, is also an indicator for the variational principle to be respected.

Using Eqs. (42) and (98) one can evaluate the potential energy contribution to the energy per particle. In addition, the knowledge of the two-body distribution function allows for the calculation of the kinetic energy per particle, to be discussed in the next Section.

5.8 Kinetic energy prescriptions

In this Section we shall perform a number of manipulations on the kinetic energy expectation value. To keep the discussion general, we do not assume that $\mathcal{F}$ takes the simple scalar Jastrow form of Eq. (20) adopted in the FR approach, but only that it is a real function of the relative particle coordinates, so that the correlator of Eq. (34) satisfies $\mathcal{F}^\dagger = \mathcal{F}$.

The kinetic energy expectation value is given by

$$\begin{aligned} \langle \hat{T} \rangle &= \frac{\hbar^2}{2m} \sum_i \langle \nabla_i^2 \rangle = A \frac{\hbar^2}{2m} \langle \nabla_1^2 \rangle \\ \langle \nabla_1^2 \rangle &= \mathrm{den}^{-1} \int dx_{1,\ldots,A} \Psi_0^* \mathcal{F}^\dagger \, \nabla_1^2 \, \mathcal{F} \Psi_0 \,, \end{aligned} \tag{99}$$

where den$= \int dx_{1,\ldots,A} \Psi_0^* \mathcal{F} \mathcal{F} \Psi_0$ accounts for the normalization of the CBF wave function In the first line we have exploited the symmetry properties of the correlated wave function, as in Eq. (41). It is worth noting that a crucial role in this context is played by the symmetryzation operator $\mathcal{S}$ appearing in Eq. (34).

The most straightforward form for the kinetic energy is obtained by applying the laplacian to the right

$$\begin{aligned}\langle\nabla_i^2\rangle_{PB} &= \mathrm{num}^{-1}\int dx_{1,\ldots,A}\Psi_0^*\mathcal{F}^\dagger(\nabla_i^2\mathcal{F}\Psi_0)\\ &= \mathrm{num}^{-1}\int dx_{1,\ldots,A}\Psi_0^*\mathcal{F}^\dagger[\mathcal{F}(\nabla_i^2\Psi_0)+2(\vec{\nabla}_i\mathcal{F})\cdot(\vec{\nabla}_i\Psi_0)+(\nabla_i^2\mathcal{F})\Psi_0]\,. \end{aligned} \tag{100}$$

This expression of the kinetic energy is called "Pandharipande-Bethe" (PB) [71], although it was first implemented by Iwamoto and Yamada [72].

The first term in square brackets generates the Fermi gas energy

$$T_F = \nu\sum_i \frac{\hbar^2 k_i^2}{2m} = A\frac{3}{5}\frac{\hbar^2 k_F^2}{2m}\,. \tag{101}$$

The full PB kinetic energy is given by

$$\langle T\rangle_{PB} = T_F + W^{kin} + W_F + U + U_F\,. \tag{102}$$

Integrals involving $\nabla_i^2 F_{ij}$ are included in W^{kin} and are completely analogous to those arising from the two-body potential. Three body terms with derivatives acting on the correlation only, $\vec{\nabla}_i F_{ij}\vec{\nabla}_i F_{ik}$, are contained in U. On the other hand, W_F and U_F accounts for the contributions coming from $\vec{\nabla}_i F_{ij}\vec{\nabla}_i \ell_{ij}$ and $\vec{\nabla}_i F_{ij}\cdot\vec{\nabla}_i \ell_{ik}$, respectively. The different contributions can be readily illustrated in the case of pure Jastrow correlations [69]

$$\begin{aligned} W^{kin} &= \frac{\rho}{2}\int d\mathbf{r}_{12}\, g(r_{12})\Big[-\frac{\hbar^2}{m}\frac{\nabla_1^2 f^c(r_{12})}{f^c(r_{12})}\Big]\\ U &= \rho^2\int d\mathbf{r}_{12}d\mathbf{r}_{13} g_3(r_{12},r_{13},r_{23})\Big[-\frac{\hbar^2}{2m}\frac{\vec{\nabla}_1 f^c(r_{12})\cdot\vec{\nabla}_1 f^c(r_{13})}{f^c(r_{12})f^c(r_{13})}\Big]\\ W_F &= \rho\int d\mathbf{r}_{12} g_{cc}(r_{12})\Big[-\frac{\hbar^2}{2m}\frac{f^{c\,\prime}(r_{12})}{f^c(r_{12})}\ell(r_{12})\Big]\\ U_F &= \rho^2\int d\mathbf{r}_{12}d\mathbf{r}_{13}\Big[-\frac{\hbar^2}{2m}\frac{f^{c\,\prime}(r_{12})}{f^c(r_{12})}\ell'(r_{13})\Big]\hat{r}_{12}\cdot\hat{r}_{13}\\ &\quad\times\sum_{exch}\{g_{cc}(r_{13})g_{dy}(r_{12})[g_{dy'}(r_{23})-1]+g_{dd}(r_{13})g_{cc}(r_{23})g_{cc}(r_{13})\}\,. \end{aligned} \tag{103}$$

In order to simplify the notation, cancellation among irreducible diagrams has been assumed; moreover, in the expression for U_F the Abe diagrams appearing in the three-body distribution function have been neglected

$$g_3(r_{12},r_{13},r_{23}) = \sum_{exch} g_{xx'}(r_{12})g_{yy'}(r_{23})g_{zz'}(r_{13})\,. \tag{104}$$

Note that terms containing $\vec{\nabla}_i\Psi_0$ gives zero contribution in direct diagrams after summation over $\mathbf{k}_i$. The only terms contributing to U_F are exchange diagrams in which $\sum_i i\mathbf{k}_i \exp(i\mathbf{k}_{ij}\cdot\mathbf{r}_{ij})$ gives $\hat{r}_{ij}\ell(r_{ij})$.

Integrating by parts the last term in square brackets of Eq. (99) and using the identity

$$\sum_i [(\vec{\nabla}_i\Psi_0^*)\mathcal{F}^\dagger(\vec{\nabla}_i\mathcal{F})\Psi_0 - \Psi_0^*(\vec{\nabla}_i\mathcal{F}^\dagger)\mathcal{F}(\vec{\nabla}_i\Psi_0)] = 0 \tag{105}$$

yields the "Clark-Westhaus" form of the kinetic energy

$$\begin{aligned}\langle\nabla_i^2\rangle_{CW} &= \mathrm{num}^{-1}\int dx_{1,\ldots,A}\Psi_0^*[\mathcal{F}^\dagger\mathcal{F}(\nabla_i^2\Psi_0) - (\vec{\nabla}_i\mathcal{F}^\dagger)\cdot(\vec{\nabla}_i\mathcal{F})\Psi_0] \\ \langle T\rangle_{CW} &= T_F + W_{CW}^{kin} - U\,. \end{aligned}\tag{106}$$

In the case of pure scalar Jastrow correlation it turns out that

$$W_{CW}^{kin} = \frac{\rho}{2}\int d\mathbf{r}_{12}\, g(r_{12})\Big[-\frac{\hbar^2}{m}\Big(\frac{f^c(r_{12})'}{f^c(r_{12})}\Big)^2\Big]\,. \tag{107}$$

Integrating once by parts the first line of Eq. (99) leads to $-(\vec{\nabla}_i\Psi_0^*\mathcal{F}^\dagger)\cdot(\vec{\nabla}_i\mathcal{F}\Psi_0)$, while yet another integration produces an expression in which the laplacian acts on the left, $(\nabla_i^2\Psi_0^*\mathcal{F}^\dagger)\mathcal{F}\Psi_0$. The Jackson-Feenberg form of the kinetic energy is obtained by averaging these contributions

$$\begin{aligned}\langle\nabla_i^2\rangle_{JF} &= \mathrm{num}^{-1}\int dx_{1,\ldots,A}\,\frac{1}{4}\Big[\Psi_0^*\mathcal{F}^\dagger(\nabla_1^2\mathcal{F}\Psi_0) - 2(\vec{\nabla}_i\Psi_0^*\mathcal{F}^\dagger)\cdot(\vec{\nabla}_1\mathcal{F}\Psi_0) \\ &\quad + (\nabla_1^2\Psi_0^*\mathcal{F}^\dagger)\mathcal{F}\Psi_0\Big] \\ \langle T\rangle_{JF} &= T_F + W_B^{kin} + W_\phi + U_\phi\,. \end{aligned}\tag{108}$$

The W_B two-body integral contains the kinetic contributions involving derivatives on correlations only ($\nabla_i^2 F_{ij} - \vec{\nabla}_i F_{ij}\cdot\vec{\nabla}_i F_{ij}$). In the case of central correlations it has the form of a two-body integral for a Bose liquid

$$W_B = \frac{\rho}{2}\int d\mathbf{r}_{12}\, g(r_{12})\Big[-\frac{\hbar^2}{2m}\Big(\frac{f^c(r_{12})\nabla_1^2 f^c(r_{12}) - f^{c\prime}(r_{12})^2}{f^c(r_{12})^2}\Big)\Big]\,. \tag{109}$$

The W_ϕ and U_ϕ have a fermionic origin as they result from $\nabla_i^2\Psi_0^*\Psi_0$ and for a scalar Jastrow correlation read

$$\begin{aligned}W_\phi &= \frac{\rho}{2\nu}\int d\mathbf{r}_{12}\Big(-\frac{\hbar^2}{2m}\Big)\Big[(g_{dd}-1)\{[\ell(r_{12}) - \nu(N_{cc}+E_{cc})]\nabla_1^2\ell(r_{12}) + \ell'(r_{12})^2\} \\ &\quad - \nu g_{dd}(r_{12})E_{cc}(r_{12})\nabla_1^2\ell(r_{12})\Big] \\ U_\phi &= \frac{\rho}{2}\int d\mathbf{r}_{12}d\mathbf{r}_{13}\Big(-\frac{\hbar^2}{4m}\Big)[(g_{dd}(r_{12})-1)\ell'(r_{12})][(g_{dd}(r_{13})-1)\ell'(r_{13})] \\ &\quad \times g_{cc}(r_{23})\hat{r}_{12}\cdot\hat{r}_{13}\,. \end{aligned}\tag{110}$$

Although the three forms of the kinetic energy that we have derived are formally equivalent, each has its own distinctive advantages and disadvantages in actual cluster expansion calculations. The CW form has the remarkable feature of not involving second derivatives and there are no additional terms arising when one goes from a Bose system to a Fermi system.

Because of the large cancellation among the two-body potential contribution and $W^{kin} + W_F$, the PB kinetic energy is rather unsensitive to the short-range uncertainties of $g_c(r_{12})$. The three body term U_ϕ of the JF procedure is smaller than the three body terms U and U_F of the PB and CW prescriptions, making the JF kinetic energy essentially unaffected by the approximations involved in the three-body distribution function. The drawback of the JF prescription mainly resides in the deficient cancellation occurring between $W_\phi + W_\phi$ and the two-body potential contribution. Hence, the JF kinetic energy is more affected by the poor knowledge of the two-body distribution function at short distances.

6 Extension to operators: FHNC/SOC

In this Section we will summarize the extension of the FR cluster expansion scheme, extensively used to deal with spin-isospin dependent correlation operators, introduced in Eq.(34)

$$\hat{\mathcal{F}}(X) = \left(\mathcal{S} \prod_{j>i=1}^{A} \hat{F}_{ij}\right) = \left(\mathcal{S} \prod_{j>i=1}^{A} \sum_{p=1}^{6} f^p(r_{ij}) \hat{O}^p_{ij}\right). \tag{111}$$

The operatorial structure of the correlations and their non commutativity make the development of a full FHNC summation scheme for diagrams containing spin-dependent correlation prohibitive. Here, we will briefly discuss the so called Single Operator Chain (FHNC/SOC) summation scheme, a detailed description of which can be found in [18, 63].

In addition to the function $h(r_{ij})$ of Eq. (38), one has to also consider the products

$$2f^c(r_{ij})f^{p>1}(r_{ij}) \quad , \quad f^{p>1}(r_{ij})f^{q>1}(r_{ij})\,. \tag{112}$$

where the factor 2 of the first quantity accounts for the term in which the central correlation is on the right of $\hat{O}^p_{12}$ while the operatorial one is on the left and for the reversed arrangement.

For the calculation of the expectation value of the NN potential depending on spin-isospin operators, like the AV18 of Eq. (2), it is worth introducing the two-body state dependent distribution functions, defined analogously to $g^c(\mathbf{r}_1, \mathbf{r}_2)$ of Eq. (40)

$$g^p(\mathbf{r}_1, \mathbf{r}_2) = \frac{A(A-1)}{\rho^2} \frac{\mathrm{Tr}_{12} \int dx_{3,\ldots,A} \Psi_0^*(X) \hat{\mathcal{F}}^\dagger \hat{O}^p_{12} \hat{\mathcal{F}} \Psi_0(X)}{\int dx_{1,\ldots,A}\ \Psi_0^*(X) \hat{\mathcal{F}}^\dagger \hat{\mathcal{F}} \Psi_0(X)}\,. \tag{113}$$

The expectation value of the two-body potential can be conveniently rewritten in terms of the two-body state dependent distribution functions

$$\langle \hat{v} \rangle \equiv \sum_{i<j} (0|\hat{v}_{ij}|0) = \frac{A(A-1)}{2} (0|\hat{v}_{12}|0) = \frac{\rho^2}{2} \sum_p \int d\mathbf{r}_{1,2}\, g^p(\mathbf{r}_1, \mathbf{r}_2) v^p(r_{12})\,. \tag{114}$$

Because of translation invariance, the state dependent distribution functions, like the scalar one, depends on the magnitude of the relative distance, $g^p(\mathbf{r}_1, \mathbf{r}_2) \equiv g^p(r_{12})$. Thus, like for the scalar case, the expectation value of the two-body potential diverges with number of particles, while

$$\frac{\langle \hat{v} \rangle}{A} = \frac{\rho}{2} \sum_p \int d\mathbf{r}_{12}\, g^p(r_{12}) v^p(r_{12}) \tag{115}$$

is a finite quantity.

Since the total spin and the total isospin of SNM are both vanishing, the following sum rules are satisfied by $g^p(r_{12})$

$$\begin{aligned} \rho \int d\mathbf{r}_{12} g^\sigma(r_{12}) &= -3 \\ \rho \int d\mathbf{r}_{12} g^\tau(r_{12}) &= -3 \\ \rho \int d\mathbf{r}_{12} g^{\sigma\tau}(r_{12}) &= 9\,. \end{aligned} \tag{116}$$

As far as the expansion of the numerator is concerned, Eq. (45) can be easily generalized

$$\hat{\mathcal{F}}^\dagger \hat{O}^p_{12} \hat{\mathcal{F}} = \hat{X}^{(2)}(x_1, x_2) + \sum_{i \neq 1,2} \hat{X}^{(3)}(x_1, x_2; x_i) + \sum_{i<j \neq 1,2} \hat{X}^{(4)}(x_1, x_2; x_i, x_j) + \dots\,. \tag{117}$$

Note that the cluster terms $\hat{X}^n$ are operators; for example

$$\begin{aligned} \hat{X}^{(2)}(x_1, x_2) &= \hat{F}^\dagger_{12} \hat{O}^p_{12} \hat{F}_{12} \\ \hat{X}^{(2)}(x_1, x_2; x_i) &= (\mathcal{S} \hat{F}^\dagger_{12} \hat{F}^\dagger_{1i} \hat{F}^\dagger_{2i}) \hat{O}^p_{12} (\mathcal{S} \hat{F}_{12} \hat{F}_{1i} \hat{F}_{2i}) - \hat{F}^\dagger_{12} \hat{O}^p \hat{F}_{12}\,. \end{aligned} \tag{118}$$

The numerator of $g^p(r_{12})$ can be expanded analogously to Eq. (49)

$$\text{num} = \sum_{N=2}^{A} \frac{\rho^{N-2}}{(N-2)!} \text{Tr}_{12} \int dx_{3,\dots,N} \hat{X}^{(N)}(x_1, x_2; x_3, \dots, x_N) \hat{g}^{MF}_N(x_1, \dots, x_N)\,, \tag{119}$$

where the operatorial $N-$body mean field distribution function, defined as

$$\hat{g}^{MF}_N(x_1, \dots, x_N) = \frac{A!}{(A-N)!} \frac{1}{\rho^N} \int dx_{N,\dots,A} \Psi_0(X)^* \Psi_0(X)\,. \tag{120}$$

can be readily shown to be (see Eq. (50) and (51))

$$\hat{g}^{MF}_N(x_1, \dots, x_N) = \frac{1}{\rho^N} \sum_{n_1,\dots,n_N} \psi^*_{n_1}(x_1) \dots \psi^*_{n_N}(x_N) \mathcal{A}[\psi_{n_1}(x_1) \dots \psi_{n_N}(x_N)]\,. \tag{121}$$

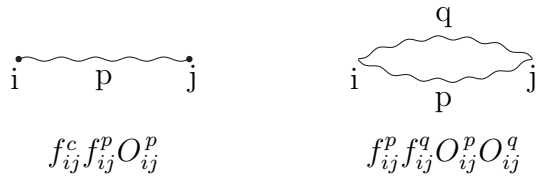

Figure 17: Operatorial correlation bonds.

The property of Eq. (52) holds for $\hat{g}_N^{MF}$, allowing for the cancellation between the unlinked diagrams of the numerator and the denominator to take place even in the case of operatorial correlations.

Writing the antisymmetrization operator as in Eq. (53) and summing over the plane wave momenta, for the first terms of $\hat{g}_N^{MF}$ we get

$$\hat{g}_N^{MF}(x_1,\ldots,x_N) = \frac{1}{\nu^N}\sum_{\alpha_i}\eta^*_{\alpha_1}\ldots\eta^*_{\alpha_N}\Big[1-\sum_{i<j}\hat{P}^{\sigma\tau}_{ij}\ell^2(r_{ij}) + \sum_{i<j<k}(\hat{P}^{\sigma\tau}_{ij}\hat{P}^{\sigma\tau}_{jk}+\hat{P}^{\sigma\tau}_{ij}\hat{P}^{\sigma\tau}_{ik})\ell(r_{ij})\ell(r_{jk})\ell(r_{ki})-\ldots\Big]\eta_{\alpha_1}\ldots\eta_{\alpha_N}\,. \tag{122}$$

This expression is very similar to the one of Eq. (62), however the sum over the spin-isospin states of the latter equation cannot be directly performed, as $\mathrm{Tr}_{1,\ldots,N}$, is not embodied in the definition of $\hat{g}_N^{MF}$.

Substituting back the expression of $\hat{g}_N^{MF}$ in Eq. (119), one finds

$$\mathrm{num} = \sum_{N=2}^{A}\frac{\rho^{N-2}}{(N-2)!}\int d\mathbf{r}_{3,\ldots,N}\mathrm{CTr}_{1,\ldots,N}\Big\{\hat{X}^{(N)}(x_1,x_2;x_3,\ldots,x_N)\Big[1-\sum_{i<j}\hat{P}^{\sigma\tau}_{ij}\ell^2(r_{ij}) + \sum_{i<j<k}(\hat{P}^{\sigma\tau}_{ij}\hat{P}^{\sigma\tau}_{jk}+\hat{P}^{\sigma\tau}_{ij}\hat{P}^{\sigma\tau}_{ik})\ell(r_{ij})\ell(r_{jk})\ell(r_{ki})-\ldots\Big]\Big\}\,. \tag{123}$$

The symbol "CTr" denotes the normalized trace of the spin-isospin operators, originating from the sum over the spin-isospin states of Eq. (122) and the sum over the spin-isospin degrees of freedom, $\mathrm{Tr}_{1,\ldots,N}$, of Eq. (119). The factor $1/\nu^N$ accounts for the normalization of the trace, such that $\mathrm{CTr}(1)=1$.

6.1 Diagrammatic rules

The diagrammatic rules given in Section 5 need to be extended to account for $2f^c(r_{ij})f^{p>1}(r_{ij})$ and $f^{p>1}(r_{ij})f^{q>1}(r_{ij})$. The former is represented by a single wavy line, the latter by a double

wavy line; in both cases a letter indicating the kind of the operator involved in the correlation is placed close to the bond itself, see Fig. 17.

A thick solid line, displayed in Fig. 18, has been introduced to represent the interaction term, $\hat{F}_{12}\hat{O}^p_{12}\hat{F}_{12}$, of the operatorial two-body distribution function.

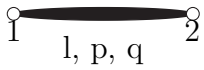

$$f^l_{12}v^p_{12}f^q_{12}\hat{O}^l_{12}\hat{O}^p_{12}\hat{O}^q_{12}$$

Figure 18: Graphical representation of an operator interaction line.

Note that the value of the diagrams in general depends on the ordering of the operators, operators; hence all permutations need to be considered.

The diagrammatic classification is analogous to the one used for the FR cluster expansion technique. As already said, disconnected diagrams of the numerator exactly simplify with the denominator and only connected diagrams have to be calculated.

Unlike the Jastrow case, reducible diagrams do not completely cancel out. At a later stage in this lecture notes, we will describe the calculation of the two- and three- body cluster contributions to the energy per particle. In those simple examples, we will show how to deal with reducible diagrams.

6.2 Traces

As can be realized from Eq. (119), the calculation of $\langle\hat{v}^p\rangle/A$ requires the evaluation of the traces of spin-isospin dependent operators present in both the potential and the correlations. Since these operators are scalar in the Fock space formed by the product of configuration, spin and isospin spaces the Pauli identity can be written as

$$(\vec{a}\cdot\vec{\sigma_i})(\vec{b}\cdot\vec{\sigma_i}) = \vec{a}\cdot\vec{b} + i\vec{\sigma_i}\cdot(\vec{a}\wedge\vec{b})\,, \tag{124}$$

where $\vec{a}$ and $\vec{b}$ are generic vector operators not containing $\vec{\sigma_i}$. The latter equation, which applies for $\vec{\sigma_i}\to\vec{\tau_i}$ also, can be used to express a generic operator product as

$$\prod\hat{O}_{ij} = C + \text{rest} \tag{125}$$

where C does not contain any spin-isospin dependent operators while the rest contains terms in which each $\vec{\sigma}_k$ and $\vec{\tau}_k$ occurs at most once. Owing to the fact that Pauli matrices are traceless

$$\mathrm{CTr}(\vec{\sigma}_k) = \mathrm{CTr}(\vec{\tau}_k) = 0\,, \tag{126}$$

the only contribution of $\prod \hat{O}_{ij}$ is C. In general C depends on the ordering of the operators appearing in $\prod \hat{O}_{ij}$, hence all the possible orderings arising from $(\mathcal{S} \prod \hat{F})$ needs to be properly taken into account.

The authors of Ref. [18] distinguished three different operatorial structures of the cluster term, to the analysis of which we devote the following Sections.

6.2.1 Product of operators acting on the same pair

As a first example, consider a cluster term in which the points i and j are joined by two operators, hence

$$\mathrm{CTr}(\hat{O}^p_{ij}\hat{O}^q_{ij}) = A^p \delta_{pq}\,, \tag{127}$$

with $A^p = 1, 3, 3, 9, 6, 18$ for $p = 1, 6$. The CTr of diagrams in which more than two operators insist on the same pair ij can be easily evaluated with the aid of the K^{pqr} matrices, defined as

$$\hat{O}^p_{ij}\hat{O}^q_{ij} = \sum_r K^{pqr}\hat{O}^r_{ij}\,. \tag{128}$$

The values of K^{pqr} are given in Table 1 of Ref. [18]. Comparing the last two equations it is readily seen that $K^{pq1} = \delta_{pq}A_p$. Using Eq. (128) it turns out that

$$\mathrm{CTr}(\hat{O}^p_{ij}\hat{O}^q_{ij}\hat{O}^r_{ij}) = \sum_s K^{pqs}\mathrm{CTr}(\hat{O}^s_{ij}\hat{O}^r_{ij}) = K^{pqr}A^r\,. \tag{129}$$

Note that, since operators acting on the same pair of points commute, the order of operator in the previous equation is immaterial, thus

$$K^{pqr}A^r = K^{qpr}A^r = K^{qrp}A^p\,\ldots \tag{130}$$

6.2.2 Single operator rings (SOR)

Single operator rings, like the one showed in Fig 19, are characterized by having at most two operators on a given point. The normalized trace of a SOR does not depend on the ordering of the operators having the point i in common. Because of the Pauli identity, the non commuting terms are indeed linear in either $\vec{\sigma_i}$ or $\vec{\tau_i}$, thus their trace vanishes.

Let $\hat{O}^p_{ij}$ and $\hat{O}^q_{jk}$ the only two operators arriving at the point j. Making use of the Pauli identity it is possible to completely eliminate the operatorial dependence on point j. Integrating over the azimuthal angle ϕ_j and tracing over the spin-isospin degrees of freedom of particle j yields

$$\mathrm{CTr}_j \int d\phi_j \hat{O}^p_{ij}\hat{O}^q_{jk} = \sum_r \int d\phi_j \xi^{pqr}_{ijk}\hat{O}^r_{ij}\,. \tag{131}$$

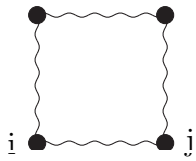

Figure 19: Four-body SOR diagram.

The coefficients ξ_{ink}^{pqr} depends on the internal angles of the triangle $\mathbf{r}_{ij}$, $\mathbf{r}_{jk}$, $\mathbf{r}_{ik}$

$$\begin{aligned}
\xi_{ijk}^{\sigma\sigma r} &= \delta_{\sigma r} \\
\xi_{ijk}^{\sigma t r} &= \delta_{tr}\frac{1}{2}(3\cos^2\theta_k - 1) \\
\xi_{ijk}^{t\sigma r} &= \delta_{tr}\frac{1}{2}(3\cos^2\theta_i - 1) \\
\xi_{ijk}^{ttr} &= \delta_{\sigma r}(3\cos^2\theta_j - 1) + \delta_{tr}\frac{1}{2}[-9\cos\theta_i\cos\theta_j\cos\theta_k \\
&\qquad - 3(\cos^2\theta_i + \cos^2\theta_j + \cos^2\theta_k) + 2] \\
\xi_{ijk}^{\tau\tau r} &= \delta_{\tau r} \\
\xi_{ijk}^{(p\tau)(q\tau)(r\tau)} &= \xi_{ijk}^{pqr}\,, \qquad p,q,r = \sigma,t.
\end{aligned} \tag{132}$$

The evaluation of SOR diagrams is rather simple: once the operators with one point in common are placed next to each other, e. g., $\hat{O}_{ij}^{p}\hat{O}_{jk}^{q}\hat{O}_{kl}^{r}\ldots$, successive contractions over the common points can be made by means of Eq. (131). Every contraction gives a ξ factor until at the end one is left with two operators acting on the same pair, resulting in a factor A^p.

6.2.3 Multiple operator diagrams

Consider the normalized trace of the diagram (a) of Fig. 20, where more than two operators arrive at both points i and j. In principle, all possible orderings of the operators have to be considered in the evaluation of the normalized trace. However, invariance under cyclic permutations is a general property of the traces. As a consequence, there are only two different orderings of the operators: a "successive" order, in which $\hat{O}_{ij}^{p}$ and $\hat{O}_{ij}^{q}$ can be placed next to each other, and an "alternate" order, in wich either $\hat{O}_{ik}^{r}$ or $\hat{O}_{jk}^{s}$ is placed between them. For the successive order, using Eq. (128), (129) and (131) it turns out that

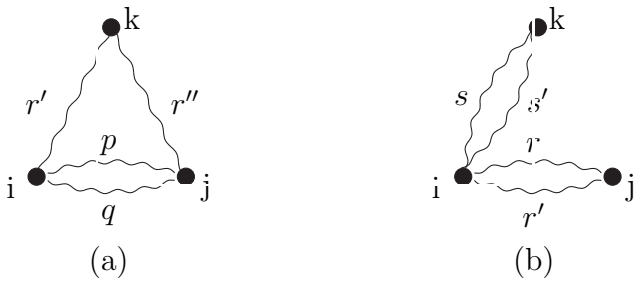

Figure 20: Multiple operator diagram

$$\begin{aligned}\int d\phi_i \mathrm{CTr}(\hat{O}^p_{ij}\hat{O}^q_{ij}\hat{O}^{r'}_{ik}\hat{O}^{r''}_{jk}) &= \sum_r K^{pqr}\int d\phi_k \mathrm{CTr}(\hat{O}^r_{ij}\hat{O}^{r'}_{ik}\hat{O}^{r''}_{jk}) \\ &= \sum_{r,r'''} K^{pqr}\int d\phi_k \xi^{r'r''r'''}_{ikj}\mathrm{CTr}(\hat{O}^r_{ij}\hat{O}^{r'''}_{ij}) \\ &= \sum_r K^{pqr}A^r\int d\phi_k \xi^{r'r''r}_{ikj}\,. \end{aligned} \tag{133}$$

On the other hand, for the alternate order one has

$$\int d\phi_i \mathrm{CTr}(\hat{O}^p_{ij}\hat{O}^{r'}_{ik}\hat{O}^q_{ij}\hat{O}^{r''}_{jk}) = \sum_r L^{pqr}\int d\phi_k \xi^{r'r''r}_{ikj}\,. \tag{134}$$

To determine the matrix L^{pqr} one has to note that either

$$\mathrm{CTr}(\hat{O}^p_{ij}[\hat{O}^{r'}_{ik},\hat{O}^q_{ij}]\hat{O}^{r''}_{jk}) = 0 \tag{135}$$

or

$$\mathrm{CTr}(\hat{O}^p_{ij}\{\hat{O}^{r'}_{ik},\hat{O}^q_{ij}\}\hat{O}^{r''}_{jk}) = 0\,. \tag{136}$$

It can be easily seen that $L^{pqr} = K^{pqr}A^r$ and $L^{pqr} = -K^{pqr}A^r$ in the former and in the latter case, respectively.

Another possibility that needs to be discussed contemplates two SOR meeting at the point i, like in the diagram (b) of Fig. 20. Because of the invariance of the trace upon cyclic exchanges, again there are only two distinct cases. When the two operators acting on the pairs ij and ik are contiguous, it turns out that

$$\mathrm{CTr}(\hat{O}^r_{ij}\hat{O}^{r'}_{ij}\hat{O}^s_{ik}\hat{O}^{s'}_{ik}) = \delta_{rr'}A^r\delta_{ss'}A^s\,, \tag{137}$$

where we have used $K^{pq1} = \delta_{pq} A_p$.

In order to deal with the alternate order, we introduce the matrix D_{rs}

$$\sum_{\vec{\sigma}_i \vec{\tau}_i} \hat{O}^r_{ij} \hat{O}^s_{ik} \hat{O}^{r'}_{ij} = \delta_{rr'} A^r (1 + D_{rs}) \hat{O}^s_{ik} \,, \tag{138}$$

where in the case of tensor operators, the above equation implies an integration over the azimuthal angle ϕ. The entries of D_{rs} depend on the kind of the operators $\hat{O}^r$ and $\hat{O}^s$

$$\begin{aligned} D_{\sigma\tau} &= 0 \quad D_{(\sigma\tau,t\tau)(\sigma\tau,t\tau)} = -\frac{8}{9} \\ D_{\sigma\sigma} &= D_{\tau\tau} = D_{(\sigma,\tau)(\sigma\tau,t\tau)} - \frac{4}{3} \,. \end{aligned} \tag{139}$$

Thus, for the alternate order trace finds

$$\mathrm{CTr}(\hat{O}^r_{ij} \hat{O}^s_{ik} \hat{O}^{r'}_{ij} \hat{O}^{s'}_{ik}) = \delta_{rr'} A^r (1 + D_{rs}) \delta_{ss'} A^s \,. \tag{140}$$

6.3 FHNC/SOC approximation

The technique for summing linked cluster diagrams containing operatorial correlations is made technically difficult because of the their non commutativity, which makes a full FHNC summation prohibitive. Diagrams having one or more passive operatorial bonds are calculated at leading order only. Such an approximation is justified by the observation that operatorial correlations are much weaker than the scalar ones. Based on this feature, one would be tempted to conclude that the leading order amounts to dressing the interaction line with all possible FHNC two-body distribution functions. This is not true as, besides the short range behavior, the intermediate range behavior of NN correlations also plays an important role that needs to be taken into account. In particular, tensor correlations, and to some extent also exchange correlations, have a much longer range than the central ones.

In order to handle this problem, summing the class of chain diagrams turns out to be to be of great importance, as remarked in Sec. 5.7 for the pure central case (see Eq. (85) and the subsequent discussion).

The above issue is taken care of by summing up the Single Operator Chains (SOC) in the corresponding FHNC/SOC approximation [18, 73]. SOC are chain diagrams in which any single passive bond of the chain has a single operator of the type $f^c(r_{ij}) f^p(r_{ij}) \hat{O}^p_{ij}$ or $-h(r_{ij}) \ell(k_F r_{ij}) \times P_{ij}$, with $p \leq 6$, or FHNC-dressed versions of them. Note that if a single bond of the chain is of the scalar type then the spin trace of the corresponding cluster term vanishes, as the Pauli matrices are traceless. Then the SOC is the leading order, and at the same time it includes the main features of the long range behavior of tensor and exchange correlations.

The calculation of SOC, as that of FHNC chains, is based upon the convolution integral of the functions corresponding to two consecutive bonds. Unlike FHNC chains, however, the SOC

have operatorial bonds. Therefore, the basic algorithm is the convolution of two operatorial correlations having one common point of Eq. (131).

The ordering of the operators within an SOC is immaterial, because the commutator $[\hat{O}_{ik}, \hat{O}_{kj}]$ is linear in $\vec{\sigma}_k$ and $\vec{\tau}_k$, and Pauli matrices are traceless. The only orderings that matter are those of passive bonds connected to the interacting points 1 or 2, discussed in Eqs. (133), (134), (137) and (140).

A second important contribution which is included in FHNC/SOC approximation is the leading order of the vertex corrections. They sum up the contributions of sets of subdiagrams which are joined to the basic diagrammatic structure in a single point, like diagram (b) of Fig. 20. Therefore, a vertex correction dresses the vertex of all the possible reducible subdiagrams joined to it. In the FHNC/SOC approximation they are taken into account only at the leading order, i.e. including SOR. Vertex corrections play an important role for the fulfillment of the sum rules.

The full FHNC/SOC equations including the SOR vertex corrections can be found in the reference paper [18, 73]. For pedagogical purposes, we limit ourselves to the equations for SOC diagrams, as this eliminates the problem of the reducible diagrams, as all the SOC diagrams are irreducible [63].

We will make the further approximation of neglecting elementary diagrams.

Regarding the notation, the symbols for nodal and composite diagrams carry an additional index, specifying the operatorial dependence: N^p_{xy}, X^p_{xy}.

The generalization of Eq. (82) accounting for operatorial nodal diagrams reads

$$N^r_{xy}(r_{12}) = \sum_{p,q=1}^{6} \sum_{x'y'} \mathrm{CTr}_3\, \rho \int_V d\mathbf{r}_3 X^p_{xx'}(r_{13}) \xi^{pqr}_{132} \zeta_{x'y'} [X^q_{y'y}(r_{23}) + N^q_{y'y}(r_{23})]\,. \tag{141}$$

Since irreducible diagrams only are present, the factor ζ_{dd} only selects contributions respecting the Pauli principle

$$\zeta_{dd} = \zeta_{de} = \zeta_{ed} = 1 \quad , \quad \zeta_{ee} = 0\,. \tag{142}$$

The partial two-body distribution functions, $g^p_{xy} = N^p_{xy} + X^p_{xy}$, are given by (compare to Eq. (93))

$$\begin{aligned}
g^p_{dd}(r_{12}) &= h^p(r_{12}) h^c(r_{12}) \\
g^p_{de}(r_{12}) &= g^p_{ed}(r_{12}) = h^c(r_{12}) [h^p(r_{12}) N^c_{de}(r_{12}) + f^c(r_{12})^2 N^p_{de}(r_{12})] \\
g^p_{ee}(r_{12}) &= h^c(r_{12}) \{ h^p(r_{12}) [N^c_{ee}(r_{12}) + N^c_{de}(r_{12})^2] - \nu f^c(r_{12})^2 \mathcal{L}(r_{12})^2 \Delta^p \\
&\quad + N^p_{ee}(r_{12}) + 2 N^c_{de}(r_{12}) N^p_{de}(r_{12}) \}\ ,
\end{aligned} \tag{143}$$

where

$$
\begin{aligned}
h^p(r_{12}) &= 2f^p(r_{12})f^c(r_{12}) + f^c(r_{12})^2 N^p_{dd}(r_{12}) \\
h^c(r_{12}) &= \exp[N_{dd}(r_{12})] \\
\mathcal{L}(r_{12}) &= N_{cc}(r_{12}) - \ell(r_{12})/\nu
\end{aligned}
\tag{144}
$$

The composite functions can be effortlessly obtained by subtracting the contribution of the nodal diagrams from the partial two-body distribution functions

$$
X^p_{xy}(r_{12}) = g^p_{xy}(r_{12}) - N^p_{xy}(r_{12})\,. \tag{145}
$$

The total operator distribution function is given by

$$
g^p(r_{12}) = g^p_{dd}(r_{12}) + 2g^p_{de}(r_{12}) + g^p_{ee}(r_{12})\,. \tag{146}
$$

Figure 21: Nodal diagrams with a cyclic exchange loop.

In a generic exchange loop all links but one carry an operator dependence. The only gap is filled by a dynamical operator to complete the operator chain. Within the SOC approximation there are two distinct possibilities: the dynamical operator may be inserted to the left (L) or to right (R) of the chain, as in the nodal diagrams (a) and (b) of Fig. 21, respectively. To deal with cyclic exchange, we need a new bond

$$
X^p_{c\,L,R}(r_{12}) = h^c(r_{12})[h^p(r_{12})\mathcal{L}(r_{12}) + f^c(r_{12})^2 N^p_{c\,L,R}(r_{12})] - N^p_{c\,L,R}(r_{12})\,, \tag{147}
$$

while the corresponding nodal functions read

$$
\begin{aligned}
N^r_{cL}(r_{12}) &= \sum_{p,q=1}^{6} \mathrm{CTr}_3\,\rho \int d\mathbf{r}_3 X^p_{c\,L}(r_{13})\xi^{pqr}_{132}\Delta^q[X_{cc}(r_{23}) + \mathcal{L}(r_{23})] \\
N^r_{cR}(r_{12}) &= \sum_{p,q=1}^{6} \mathrm{CTr}_3\,\rho \int \mathbf{r}_3 X_{cc}(r_{13})\Delta^p\xi^{pqr}_{132}[X^q_{c\,R}(r_{13}) + N^q_{c\,R}(r_{13})] \\
N^r_{cc}(r_{12}) &= N^r_{cL}(r_{12}) + N^r_{cR}(r_{12})\,.
\end{aligned}
\tag{148}
$$

Finally, the partial two-body distribution functions with circular exchanges is given by

$$g_c^p(r_{12}) = g_{cc}^c(r_{12})\Delta^p \,. \tag{149}$$

The *cc* nodal functions enter as closed SOR in the generalized equations for X_{ee}^c and N_{cc}^c. Moreover, they contribute to the energy expectation value, the full calculation of which will not be reported in this lecture notes. The interested reader is again referred to the Refs. [18, 73]. Nevertheless, in the next Section, we do present the calculation of the two- and three- body cluster contributions to both the potential and the kinetic energy per particle.

6.4 Two- and three- body cluster contribution

In this Section we analyze in detail the two- and the three- body cluster contributions to the energy per particle for the case of a "static" potential, without momentum dependent terms. This analysis, although being useful for pedagogical reasons, in particular for the treatment of the reducible diagrams within the FR summation scheme, will be the cornerstone of the effective interaction, that will be developed for the calculation of the response.

With the notation used in Section 6, the two-body contribution of $\mathcal{F}^\dagger v_{12}\mathcal{F}$ can be expressed as

$$\mathcal{F}^\dagger v_{12}\mathcal{F}\Big|_{2b} \equiv \hat{X}^2(x_1,x_2) = \hat{F}_{12}\hat{v}_{12}\hat{F}_{12}\,. \tag{150}$$

In what follows, the cluster expansion of the denominator will be disregarded as it is understood that, for fermionic systems, the denominator exactly cancels the disconnected diagrams of the numerator.

The two-body contribution of the potential is then

$$\begin{aligned}\langle\hat{v}\rangle\Big|_{2b} &= \frac{1}{2}\sum_{n_1,n_2}\int dx_1dx_2\phi^*_{n_1}(x_1)\phi^*_{n_2}(x_2)\hat{F}_{12}\hat{v}_{12}\hat{F}_{12}(1-\hat{P}_{12})\phi_{n_1}(x_1)\phi_{n_2}(x_2)\\ &= \frac{\rho^2}{2}\int d\mathbf{r}_1d\mathbf{r}_2\mathrm{CTr}_{12}[\hat{F}_{12}\hat{v}_{12}\hat{F}_{12}(1-\hat{P}_{12}^{\sigma\tau}\ell_{12}^2)]\,.\end{aligned} \tag{151}$$

Because of the translation invariance of the system, it is possible to integrate out the coordinate of the center of mass $\mathbf{R}_{12} = \frac{1}{2}(\mathbf{r}_1+\mathbf{r}_2)$, so that the two-body cluster contribution to the potential energy per particle reads

$$\frac{\langle\hat{v}\rangle}{A}\Big|_{2b} = \frac{\rho}{2}\int d\mathbf{r}_{12}\,\mathrm{CTr}_{12}[\hat{F}_{12}\hat{v}_{12}\hat{F}_{12}(1-\hat{P}_{12}^{\sigma\tau}\ell_{12}^2)]\,. \tag{152}$$

The two-body term of the cluster expansion of the kinetic energy, $\hat{T}$, is

$$-\frac{\hbar^2}{2m}\nabla_1^2\mathcal{F}^\dagger\mathcal{F}\Big|_{2b} \equiv \sum_{1<i}\hat{X}^2(x_1;x_i) = \sum_{1<i}^{A}\Big(-\frac{\hbar^2}{2m}\hat{F}_{1i}[\nabla_1^2,\hat{F}_{1i}]\Big)\,, \tag{153}$$

where the commutator removes the Fermi gas energy, which is a one-body contribution. Using the symmetry of the wave functions one gets

$$\langle \hat{T} \rangle \Big|_{2b} = -\frac{\hbar^2}{2m} \sum_{n_1,n_2} \int dx_1 dx_2 \phi^*_{n_1}(x_1) \phi^*_{n_2}(x_2) \hat{F}_{12} [\nabla_1^2, \hat{F}_{12}] (1 - \hat{P}_{12}) \phi_{n_1}(x_1) \phi_{n_2}(x_2) \,. \tag{154}$$

In order to remove the term with the product of the gradients acting on both the correlation function $\hat{F}_{12}$ and on the plane wave, it is convenient to integrate by part the latter expression (see Section 5.8), with the result

$$\langle \hat{T} \rangle \Big|_{2b} = \frac{\hbar^2}{2m} \sum_{n_1,n_2} \int dx_1 dx_2 \phi^*_{n_1}(x_1) \phi^*_{n_2}(x_2) (\vec{\nabla}_1 \hat{F}_{12}) (\vec{\nabla}_1 \hat{F}_{12}) (1 - \hat{P}_{12}) \phi_{n_1}(x_1) \phi_{n_2}(x_2) \,. \tag{155}$$

Since $\vec{\nabla}_1 \hat{F}_{12} = \vec{\nabla}_{12} \hat{F}_{12}$, we can integrate out the coordinate of the center of mass, getting the following expression for the kinetic energy per particle

$$\frac{\langle \hat{T} \rangle}{A} \Big|_{2b} = \frac{\hbar^2}{2m} \rho \int d\mathbf{r}_{12} \, \mathrm{CTr}_{12} [(\vec{\nabla}_{12} \hat{F}_{12}) (\vec{\nabla}_{12} \hat{F}_{12}) (1 - \hat{P}_{12}^{\sigma\tau} \ell_{12}^2)] \,. \tag{156}$$

For calculating $(\vec{\nabla}_1 \hat{F}_{12})(\vec{\nabla}_1 \hat{F}_{12})$ one has to account for the fact that the tensor operator depends on $\hat{r}_{12}$, hence

$$\begin{aligned} (\vec{\nabla}_1 \hat{F}_{12})(\vec{\nabla}_1 \hat{F}_{12}) &= \sum_{p,q} [(\vec{\nabla}_1 f_{12}^p) \hat{O}_{12}^p + f_{12}^p (\vec{\nabla}_1 \hat{O}_{12}^p)][(\vec{\nabla}_1 f_{12}^q) \hat{O}_{12}^q + f_{12}^q (\vec{\nabla}_1 \hat{O}_{12}^q)] \\ &= \sum_{p,q} [(\vec{\nabla}_1 f_{12}^p) \hat{O}_{12}^p (\vec{\nabla}_1 f_{12}^q) \hat{O}_{12}^q + f_{12}^p (\vec{\nabla}_1 \hat{O}_{12}^p) f_{12}^q (\vec{\nabla}_1 \hat{O}_{12}^q)] \,, \end{aligned} \tag{157}$$

where the following property of the gradient of the tensor operator has been used

$$\vec{\nabla}_1 f(r_{12}) \vec{\nabla}_1 S_{12} = 0 \,. \tag{158}$$

The first term of Eq. (157) can be conveniently written in terms of the derivative with respect the magnitude of $\mathbf{r}_{12}$

$$\sum_{p,q} (\vec{\nabla}_1 f_{12}^p) \hat{O}_{12}^p (\vec{\nabla}_1 f_{12}^q) \hat{O}_{12}^q = \sum_{p,q} f_{12}'^p \, \hat{O}_{12}^p \, f_{12}'^q \, \hat{O}_{12}^q \,. \tag{159}$$

Thanks to the relation

$$(\vec{\nabla}_1 S_{12})(\vec{\nabla}_1 S_{12}) = \frac{6}{r_{12}^2} (6 + 2\sigma_{12} + S_{12}) \,, \tag{160}$$

the second term of Eq. (157) turns out to be

$$\sum_{p,q} [f_{12}^p (\vec{\nabla}_1 \hat{O}_{12}^p) f_{12}^q (\vec{\nabla}_1 \hat{O}_{12}^q)] = \frac{6}{r_{12}^2} (f_{12}^t + f_{12}^{t\tau} \tau_{12})^2 (6 + 2\sigma_{12} + S_{12}) \tag{161}$$

The three-body cluster contribution appearing in the expansion of $\mathcal{F}^\dagger v_{12}\mathcal{F}$ is given by

$$\begin{aligned}\mathcal{F}^\dagger v_{12}\mathcal{F}\Big|_{3b} &= \sum_{i>2}\hat{X}^3(x_1,x_2;x_i)\\ &= \sum_{i>2}\Big[\Big(\mathcal{S}\hat{F}_{12}\hat{F}_{1i}\hat{F}_{2i}\Big)\hat{v}_{12}\Big(\mathcal{S}\hat{F}_{12}\hat{F}_{1i}\hat{F}_{2i}\Big)-\hat{F}_{12}\hat{v}_{12}\hat{F}_{12}\Big]\,. \end{aligned} \tag{162}$$

Within the FR diagrammatic scheme, the three-body cluster contribution to $\langle\hat{v}_{12}\rangle$ it is not merely the expectation value of the latter result, unlike the two-body case. As a matter of fact, the reducible diagrams arising form four-body cluster term of $\mathcal{F}^\dagger v_{12}\mathcal{F}$, the detailed calculations of which can be found in appendix B, needs to be taken into account.

The direct term of the three-body cluster contribution in the FR expansion scheme is given by [64]

$$\begin{aligned}\langle\hat{v}_{12}\rangle\Big|_{3b}^{\rm dir} = \frac{\rho^2}{2}\int d\mathbf{r}_{12}d\mathbf{r}_{13}\mathrm{CTr}_{123}\Big[&(\mathcal{S}\hat{F}_{12}\hat{F}_{13}\hat{F}_{23})\hat{v}_{12}(\mathcal{S}\hat{F}_{12}\hat{F}_{13}\hat{F}_{23})\\ &-\hat{F}_{12}\hat{v}_{12}\hat{F}_{12}(\hat{F}_{13}^2+\hat{F}_{23}^2-1)\Big]\,.\end{aligned} \tag{163}$$

It includes the term

$$(\mathcal{S}\hat{F}_{12}\hat{F}_{13}\hat{F}_{23})\hat{v}_{12}(\mathcal{S}\hat{F}_{12}\hat{F}_{13}\hat{F}_{23})-\hat{F}_{12}\hat{v}_{12}\hat{F}_{12} \tag{164}$$

from the three-body cluster contribution of $\mathcal{F}^\dagger v_{12}\mathcal{F}$, whereas the reducible four-body diagrams of Fig. 22 contribute with the factor

$$-\hat{F}_{12}\hat{v}_{12}\hat{F}_{12}(\hat{F}_{13}^2+\hat{F}_{23}^2-2)\,. \tag{165}$$

It is worth remarking that in the pure central Jastrow case, $\hat{F}_{ij}=f_{ij}^c$, the four- and three-body reducible diagrams completely cancel, as discussed in Section 5.6, and we obtain the well-known irreducible contribution

$$\langle\hat{v}_{12}\rangle\Big|_{3b}^{\text{dir-Jastrow}} = \frac{\rho^2}{2}\int d\mathbf{r}_{12}d\mathbf{r}_{13}f^{c2}(r_{12})v(r_{12})(f^{c2}(r_{13})-1)(f^{c2}(r_{23})-1)\,. \tag{166}$$

The sum of the diagrams where particles 1 and 2 are exchanged gives

$$\begin{aligned}\langle\hat{v}_{12}\rangle\Big|_{3b}^{P_{12}} = -\frac{\rho^2}{2}\int d\mathbf{r}_{12}d\mathbf{r}_{13}\ell^2(r_{12})\mathrm{CTr}_{123}\Big[&(\mathcal{S}\hat{F}_{12}\hat{F}_{13}\hat{F}_{23})\hat{v}_{12}(\mathcal{S}\hat{F}_{12}\hat{F}_{13}\hat{F}_{23})\hat{P}_{12}^{\sigma\tau}\\ &-\hat{F}_{12}\hat{v}_{12}\hat{F}_{12}(\hat{F}_{13}^2+\hat{F}_{23}^2-1)\hat{P}_{12}^{\sigma\tau}\Big]\,.\end{aligned} \tag{167}$$

The corresponding four-body diagram producing the term $\frac{1}{2}\hat{F}_{12}\hat{v}_{12}\hat{F}_{12}(\hat{F}_{13}^2+\hat{F}_{23}^2-2)\hat{P}_{12}^{\sigma\tau}$ is drawn in Fig. 23

The diagrams in which particles 1 and 3 are exchanged contributes with

$$\langle \hat{v}_{12} \rangle \Big|_{3b}^{P_{13}} = -\frac{\rho^2}{2} \int d\mathbf{r}_{12} d\mathbf{r}_{13} \ell^2(r_{13}) \mathrm{CTr}_{123} \Big[(\mathcal{S}\hat{F}_{12}\hat{F}_{13}\hat{F}_{23}) \hat{v}_{12} (\mathcal{S}\hat{F}_{12}\hat{F}_{13}\hat{F}_{23}) \hat{P}_{13}^{\sigma\tau} - \hat{F}_{12}\hat{v}_{12}\hat{F}_{12}\hat{F}_{13}^2\hat{P}_{13}^{\sigma\tau} \Big] . \quad (168)$$

where the term $\frac{1}{2}\hat{F}_{12}\hat{v}_{12}\hat{F}_{12}(\hat{F}_{13}^2 - 1)\hat{P}_{13}^{\sigma\tau}$ comes from the four-body reducible diagram of Fig. 24.

Since the potential is invariant under $x_1 \leftrightarrow x_2$. the diagrams with the exchange between particles 2 and 3 give the same contribution reported in Eq. (168). The associated four-body reducible diagram is very similar to the one of Fig. 24 but with the loop attached to particle 2 instead of particle 1.

Consider the diagrams with the circular exchange involving particles 1, 2 and 3. In this case there are no reducible four-body diagrams that partly cancel the reducible part of the three body diagram. In addition, there are no three-body reducible diagrams with circular exchange at all. However, the four-body diagram of Fig. 24, with no correlation lines linking particles 1 and 2 to the others, can be *reduced* to a three-body term, so that the three-body

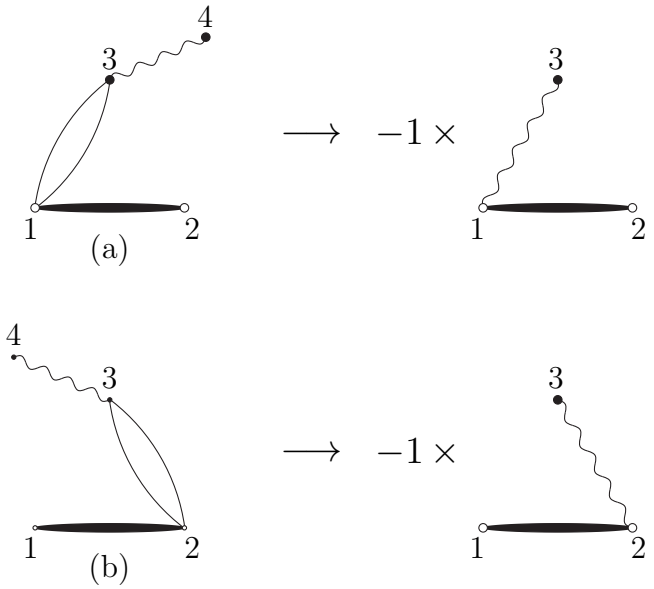

Figure 22: Four-body reducible diagrams, $v_{4b\to 3b}^{\mathrm{dir}}$ and their three-body reduction.

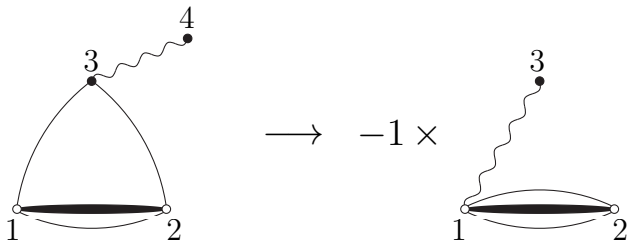

Figure 23: Four-body reducible diagram, $v^{\mathrm{P12}}_{4b\to 3b}$, and its three-body reduction.

diagram with a circular exchange reads

$$\langle \hat{v}_{12} \rangle \Big|^{cir}_{3b} = \rho^2 \int d\mathbf{r}_{12} d\mathbf{r}_{13} \ell(r_{12}) \ell(r_{13}) \ell(r_{23}) \mathrm{CTr}_{123} \Big[(\mathcal{S}\hat{F}_{12}\hat{F}_{13}\hat{F}_{23}) \hat{v}_{12} (\mathcal{S}\hat{F}_{12}\hat{F}_{13}\hat{F}_{23}) \hat{P}^{\sigma\tau}_{12} \hat{P}^{\sigma\tau}_{13} - \hat{F}_{12}\hat{v}_{12}\hat{F}_{12}\hat{F}^2_{13}\hat{P}^{\sigma\tau}_{13}\hat{P}^{\sigma\tau}_{12} \Big] . \tag{169}$$

As explained in Section 5.8, three-body cluster contribution to the PB kinetic energy contains terms of the kind $\nabla^2_1(\mathcal{S}\hat{F}_{12}\hat{F}_{13}\hat{F}_{23})$. Their explicit expressions can be obtained from the corresponding equations for the two-body potential by substituting the first term of the normalized traces with

$$\hat{v}_{12}(\mathcal{S}\hat{F}_{12}\hat{F}_{13}\hat{F}_{23}) \to -2[\mathcal{S}(\nabla^2_1\hat{F}_{12})\hat{F}_{13}\hat{F}_{23}] - 2[\mathcal{S}(\vec{\nabla}_1\hat{F}_{12})\cdot(\vec{\nabla}_1\hat{F}_{13})\hat{F}_{23}] , \tag{170}$$

while

$$\hat{v}_{12}\hat{F}_{12} \to -2(\nabla^2_1\hat{F}_{12}) \tag{171}$$

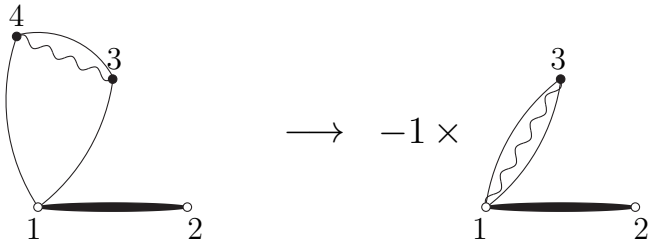

Figure 24: Four-body reducible diagram, $v^{\mathrm{P13}}_{4b\to 3b}$, and its three-body reduction.

for the second term. Following the notation of Section 5.8, terms with $(\nabla_1^2 \hat{F}_{12})$ are denoted by W^{kin}, those having $(\vec{\nabla}_1 \hat{F}_{12}) \cdot (\vec{\nabla}_1 \hat{F}_{13})$ are included in U. On the other hand, the three-body cluster terms belonging to W_F arise from the diagrams where particles 1 and 2 are exchanged

$$\langle \hat{T} \rangle \Big|_{3b\,W_F}^{P_{12}} = \frac{\hbar^2}{m} \rho^2 \int d\mathbf{r}_{12} d\mathbf{r}_{13} \ell(r_{12}) \ell'(r_{12}) \hat{r}_{12} \cdot \mathrm{CTr}_{123} \Big[(\mathcal{S} \hat{F}_{12} \hat{F}_{13} \hat{F}_{23}) \times \\ [\mathcal{S}(\vec{\nabla}_1 \hat{F}_{12}) \hat{F}_{13} \hat{F}_{23}) \hat{P}_{12}^{\sigma\tau} - \hat{F}_{12} (\vec{\nabla}_1 \hat{F}_{12}) (\hat{F}_{13}^2 + \hat{F}_{23}^2 - 1) \hat{P}_{12}^{\sigma\tau} \Big] \tag{172}$$

and from the ones with circular exchange

$$\langle \hat{T} \rangle \Big|_{3b\,W_F}^{cir} = -\frac{\hbar^2}{m} \rho^2 \int d\mathbf{r}_{12} d\mathbf{r}_{13} \ell(r_{13}) \ell(r_{23}) \ell'(r_{12}) \hat{r}_{12} \cdot \mathrm{CTr}_{123} \Big[(\mathcal{S} \hat{F}_{12} \hat{F}_{13} \hat{F}_{23}) \\ [\mathcal{S}(\vec{\nabla}_1 \hat{F}_{12}) \hat{F}_{13} \hat{F}_{23}] \hat{P}_{12}^{\sigma\tau} \hat{P}_{13}^{\sigma\tau} - \hat{F}_{12} (\vec{\nabla}_1 \hat{F}_{12}) \hat{F}_{13}^2 \hat{P}_{13}^{\sigma\tau} \hat{P}_{12}^{\sigma\tau} \Big] . \tag{173}$$

The contributions to U stem from the diagrams with the exchange P_{13}

$$\langle \hat{T} \rangle \Big|_{3b\,U_F}^{P_{13}} = \frac{\hbar^2}{m} \rho^2 \int d\mathbf{r}_{12} d\mathbf{r}_{13} \ell'(r_{13}) \hat{r}_{13} \cdot \mathrm{CTr}_{123} \Big[(\mathcal{S} \hat{F}_{12} \hat{F}_{13} \hat{F}_{23}) \times \\ [\mathcal{S}(\vec{\nabla}_1 \hat{F}_{12}) \hat{F}_{13} \hat{F}_{23}) \hat{P}_{13}^{\sigma\tau} \Big] \tag{174}$$

and from those having circular exchange

$$\langle \hat{T} \rangle \Big|_{3b\,U_F}^{cir} = -\frac{\hbar^2}{m} \rho^2 \int d\mathbf{r}_{12} d\mathbf{r}_{13} \ell(r_{12}) \ell(r_{13}) \ell'(r_{13}) \hat{r}_{23} \cdot \mathrm{CTr}_{123} \Big[(\mathcal{S} \hat{F}_{12} \hat{F}_{13} \hat{F}_{23}) \\ [\mathcal{S}(\vec{\nabla}_1 \hat{F}_{12}) \hat{F}_{13} \hat{F}_{23}] \hat{P}_{12}^{\sigma\tau} \hat{P}_{13}^{\sigma\tau} \Big] . \tag{175}$$

Note that in this case there are no subtraction terms arising from reducible diagrams.

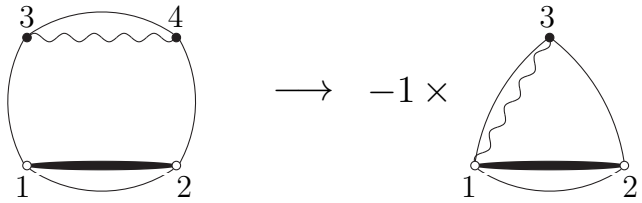

Figure 25: Four-body diagram, $v_{4b\to 3b}^{\mathrm{cir}}$, that contributes to the three-body diagrams having a circular exchange between particles 1, 2 and 3.

6.5 Determination of the correlation functions

An upperbound to the binding energy per particle, E_V/A, can be obtained by using the variational method, which amounts to minimizing the energy expectation value $\langle H\rangle/A$ with respect to the variational parameters included in the model. Its cluster expansion is given by

$$\frac{\langle H\rangle}{A} = T_F + (\Delta E)_2 + \text{higher order terms}\,, \tag{176}$$

where T_F is the energy of the non interacting Fermi gas and $(\Delta E)_2$ denotes the contribution of two-nucleon clusters

$$(\Delta E)_2 = \mathcal{F}^\dagger v_{12}\mathcal{F}\Big|_{2b} + \langle\hat{T}\rangle\Big|_{2b}\,. \tag{177}$$

Neglecting higher order cluster contributions, the functional minimization of $\langle H\rangle/A$ leads to a set of six Euler-Lagrange equations, to be solved with proper constraints that force f^c and $f^{(p>1)}$ to "heal" at one and zero, respectively. That is most efficiently achieved through the boundary conditions [74, 18]

$$\begin{aligned} f^p(r \geq d^p) &= \delta_{p1}\,, \\ \frac{df^p(r)}{dr}\,|_{d^p} &= 0\,. \end{aligned} \tag{178}$$

Numerical calculations are generally carried out using only two independent "healing distances": $d_c = d^{p=1\ldots4}$ and $d_t = d^{5,6}$.

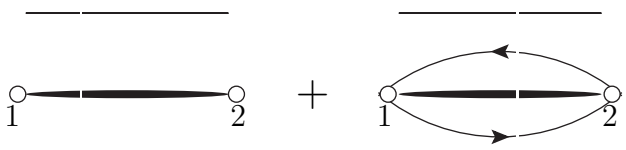

Figure 26: Diagrammatic representation of the two-body cluster contribution $(\Delta E)_2$ of Eq. (176). The thick lines represents both the potential and a kinetic contribution, involving derivatives acting only on the correlation functions. The effect of the other derivatives is included in T_F.

Additional and important variational parameters are the quenching factors α_p whose introduction simulates modifications of the two–body potentials entering in the Euler–Lagrange differential equations arising from the screening induced by the presence of the nuclear medium

$$\hat{v}_{ij} = \sum_{p=1}^{6} \alpha_p v^p(r_{ij})\hat{O}^p_{ij}\,. \tag{179}$$

The full potential is, of course, used in the energy expectation value. In addition, the resulting correlation functions f^p are often rescaled according to

$$\hat{F}_{ij} = \sum_{p=1}^{6} \beta_p f^p(r_{ij}) \hat{O}^p_{ij} \, , \tag{180}$$

The energy expectation value $\langle H \rangle / A$, calculated in full FHNC/SOC approximation is minimized with respect to variations of d_c, d_t, β_p, and α_p.

To determine the best values of the variational parameters we have used a version of the "Simulated annealing" algorithm [75]. In metallurgy the annealing procedure consists in heating and then slowly cooling a metal, to decrease the defects of its structure. During the heating the atoms gain kinetic energy and move away from their initial equilibrium positions, passing through states of higher energy. Afterwards, when the metal slowly cools, it is possible that the atoms freeze in a different configuration with respect to the initial one, corresponding to a lower value of the energy.

In minimization problems the analog of the position of the atoms are the values of the parameters to be optimized, in our case d_c, d_t, β_p and α_p, while the energy of the system corresponds to the function that has to be minimized, that in our case is the variational energy

$$E_V = E_V(d_c, d_t, \beta_p, \alpha_p) \, . \tag{181}$$

In the simulated annealing procedure, the parameters d_c, d_t, β_p, α_p are drawn from the Boltzmann distribution, $\exp(-E_V/T)$, where T is just a parameter of the simulated annealing algorithm, having no physical meaning.

We have used a Metropolis algorithm, with acceptance probability of passing from the state $s = \{d_c, d_t, \beta_p, \alpha_p\}$ to the proposed state $s' = \{d'_c, d'_t, \beta'_p, \alpha'_p\}$ given by

$$P_{s,s'} = \exp\Big[- \frac{E(s') - E(s)}{T} \Big] \, , \tag{182}$$

By looking at the distribution of the parameters resulting from the Metropolis random walk, it is possible to find the values $\tilde{d}_c$, $\tilde{d}_t$, $\tilde{\beta}_p$ and $\tilde{\alpha}_p$ corresponding to the minimum of E_V, e.g. to the maximum of the Boltzmann distribution. As the fictitious temperature T is lowered, the system approaches the equilibrium and the values of the parameters get closer and closer to $\tilde{d}_c$, $\tilde{d}_t$, $\tilde{\beta}_p, \tilde{\alpha}_p$.

A The Hartree-Fock method

The starting point to derive the Hartree-Fock equation is the variational principle

$$E_0 \leq E[\Psi] = \langle \Psi | H | \Psi \rangle \,, \tag{183}$$

valid when the Slater determinant has been normalized to unity. At this aim we require that single particle wave functions be orthonormal

$$\int dx\, \psi_{n_i}(x) \psi_{n_j}(x) = \delta_{n_i n_j} \,. \tag{184}$$

It is straightforward to show [76] that the expectation value of the Hamiltonian is made of three contributions

$$E[\Psi] = \sum_{n_i=1}^{A} I_{n_i} + \frac{1}{2} \sum_{n_i,n_j=1}^{A} \left[J_{n_i n_j} - K_{n_i n_j} \right] . \tag{185}$$

The first contribution comes from the kinetic energy, as no genuine one-body potential appears in the nuclear Hamiltonian of Eq. (1)

$$I_{n_i} = \int dx_i \psi^*_{n_i}(x_i) \frac{\nabla_i^2}{2m} \psi_{n_i}(x_i) \,, \tag{186}$$

while the direct term $J_{n_i n_j}$ and the exchange term $K_{n_i n_j}$ arise from the two-body potential

$$\begin{aligned} J_{n_i n_j} &= \int dx_i dx_j \psi^*_{n_i}(x_i) \psi^*_{n_j}(x_j) v_{ij} \psi_{n_i}(x_i) \psi_{n_j}(x_j) \\ K_{n_i n_j} &= \int dx_i dx_j \psi^*_{n_i}(x_i) \psi^*_{n_j}(x_j) v_{ij} \psi_{n_j}(x_i) \psi_{n_i}(x_j) \,. \end{aligned} \tag{187}$$

The variational principle is applied by requiring that the functional $E[\Psi]$ being stationary upon variations of the A occupied spin-orbitals ψ_{n_i}, with the constraint that the spin-orbitals must remain orthogonal. To achieve this, a set of A^2 Lagrange multipliers ϵ_{n_i,n_j} is introduced in the variational equation

$$\delta E[\Psi] - \sum_{n_i,n_j=1}^{A} \epsilon_{n_i,n_j} \, \delta \Big[\int dx_i \psi^*_{n_i}(x_i) \psi_{n_j}(x_i) \Big] = 0 \,. \tag{188}$$

Since the energy is a real quantity, the Lagrange multipliers are elements of an Hermitian matrix, $\epsilon_{n_i n_j} = \epsilon^*_{n_j n_i}$.

The matrix of the Lagrange multipliers can therefore be diagonalized performing a unitary transformation on the spin-orbitals

$$\psi'_{n_i} = \sum_{n_j} U_{n_i,n_j} \psi_{n_j} \,. \tag{189}$$

The new Slater determinant differs by a phase factor from the previous one, $\Psi' = det(U)\Psi$, while the functional $E[\psi]$ is not affected by this unitary transformation.

To simplify the notation, instead of working with the primed indeces, we assume that the diagonalization has been made from the beginning. Therefore Eq. (188) can be written as

$$\delta E[\Psi] - \sum_{n_i} \epsilon_{n_i}\, \delta\Big[\int dx_i \psi^*_{n_i}(x_i)\psi_{n_i}(x_i)\Big] = 0\,, \tag{190}$$

being $\{\epsilon_{n_i}\}$ the eigenvalues of $\epsilon_{n_i n_j}$.

Carrying out the variation $\delta E[\Psi]$ leads to the canonical set of integro-differential Hartree Fock equations

$$\Big(-\frac{\nabla^2}{2m} + \sum_{n_j}[\hat{J}_{n_j} - \hat{K}_{n_j}]\Big)\psi_{n_i}(x_i) = \epsilon_{n_i}\psi_{n_i}(x_i)\,. \tag{191}$$

The direct and exchange operators, $\hat{J}$ and $\hat{K}$, respectively, result from the differentiation of the direct and of the exchange term defined in Eq. (187). While the direct operator is local

$$\hat{J}_{n_j}\psi_{n_i}(x_i) = \int dx_j \psi^*_{n_j}(x_j) v_{ij} \psi_{n_j}(x_j)\psi_{n_i}(x_i)\,, \tag{192}$$

as in order to evaluate their action on a given function at a point in the configurational space, we need to know just the value of the function at the same point. On the other hand, the exchange operator

B Four-body reducible diagrams

In this appendix we report the explicit calculations of the four-body reducible diagrams involved in the calculations of the FR three-body cluster contribution of $\langle v_{12}\rangle$.

The analytic expression of diagram (a) drawn in Fig. 22 is

$$v^{\rm dir\ (a)}_{4b\to 3b} = -\frac{\rho^4}{2A}\int d\mathbf{r}_{1234}\ell^2(r_{13})\mathrm{CTr}_{1234}\Big[\hat{F}_{12}v_{12}\hat{F}_{12}(\hat{F}^2_{34}-1)\hat{P}_{13}\Big]\,. \tag{193}$$

Because of the tracing over the spin-isospin variables of particle 4, only the central part of $\hat{F}^2_{34}$ does not vanish; hence, only the scalar part of the exchange operator survives

$$\begin{aligned} v^{\rm dir\ (a)}_{4b\to 3b} &= -\frac{\rho^4}{2A}\frac{1}{\nu}\int d\mathbf{r}_{1234}\ell^2(r_{13})\mathrm{CTr}_{1234}\Big[\hat{F}_{12}v_{12}\hat{F}_{12}(\hat{F}^2_{34}-1)\Big] \\ &= -\frac{\rho^3}{2}\frac{1}{\nu}\int d\mathbf{r}_{12}d\mathbf{r}_{13}d\mathbf{r}_{34}\ell^2(r_{13})\mathrm{CTr}_{1234}\Big[\hat{F}_{12}v_{12}\hat{F}_{12}(\hat{F}^2_{34}-1)\Big] \\ &= -\frac{\rho^2}{2}\int d\mathbf{r}_{12}d\mathbf{r}_{34}\mathrm{CTr}_{1234}\Big[\hat{F}_{12}v_{12}\hat{F}_{12}(\hat{F}^2_{34}-1)\Big]\,, \end{aligned} \tag{194}$$

where we have used

$$\int d\mathbf{r}_{12}\ell^2(r_{12}) = \frac{\nu}{\rho} \tag{195}$$

Renaming the integration variables yields to the expression entering Eq. (163)

$$v_{4b\to 3b}^{\text{dir (a)}} = -\frac{\rho^2}{2}\int d\mathbf{r}_{12}d\mathbf{r}_{13}\text{CTr}_{123}\Big[\hat{F}_{12}v_{12}\hat{F}_{12}(\hat{F}_{13}^2-1)\Big]\,. \tag{196}$$

The calculation of diagram (b) of Fig. 22 follows analogously.

The contribution of the diagram depicted in Fig. 23 is given by

$$v_{4b\to 3b}^{\text{P12}} = \frac{\rho^4}{A}\int d\mathbf{r}_{1234}\ell(r_{12})\ell(r_{13})\ell(r_{23})\text{CTr}_{1234}\Big[\hat{F}_{12}v_{12}\hat{F}_{12}(\hat{F}_{34}^2-1)\hat{P}_{12}\hat{P}_{13}\Big]\,. \tag{197}$$

As before, since only the central part of $\hat{F}_{34}^2$ survives, it turns out that

$$v_{4b\to 3b}^{\text{P12}} = \frac{\rho^4}{A}\frac{1}{\nu}\int d\mathbf{r}_{1234}\ell(r_{12})\ell(r_{13})\ell(r_{23})\text{CTr}_{1234}\Big[\hat{F}_{12}v_{12}\hat{F}_{12}(\hat{F}_{34}^2-1)\hat{P}_{12}\Big]\,. \tag{198}$$

Thanks to the property

$$\int d\mathbf{r}_{13}\ell(r_{13})\ell(|\mathbf{r}_{12}-\mathbf{r}_{13}|) = \frac{\nu}{\rho}\ell(r_{12})\,, \tag{199}$$

and relabeling the integration variables, one arrives to the following expression

$$v_{4b\to 3b}^{\text{p12}} = \rho^2\int d\mathbf{r}_{12}d\mathbf{r}13\ell(r_{12})^2\text{CTr}_{123}\Big[\hat{F}_{12}v_{12}\hat{F}_{12}(\hat{F}_{13}^2-1)\hat{P}_{12}\Big]\,. \tag{200}$$

Notice that, to recover the contribution to Eq. (167), one the symmetry $1 \leftrightarrow 2$ needs to be exploited.

Let us now consider the diagram of Fig. 24

$$v_{4b\to 3b}^{\text{p13}} = \frac{\rho^4}{2A}\int d\mathbf{r}_{1234}\ell(r_{13})\ell(r_{14})\ell(r_{34})\text{CTr}_{1234}\Big[\hat{F}_{12}v_{12}\hat{F}_{12}(\hat{F}_{34}^2-1)\hat{P}_{13}\hat{P}_{34}\Big]\,. \tag{201}$$

Carrying out the trace over spin-isospin variables of particle 4 makes only the central part of $(\hat{F}_{34}^2-1)\hat{P}_{34}$ not to vanish. Hence only the scalar part of $\hat{P}_{13}$ contributes

$$\begin{aligned} v_{4b\to 3b}^{\text{p13}} &= \frac{\rho^4}{2A}\frac{1}{\nu}\int d\mathbf{r}_{1234}\ell(r_{13})\ell(r_{14})\ell(r_{34})\text{CTr}_{1234}\Big[\hat{F}_{12}v_{12}\hat{F}_{12}(\hat{F}_{34}^2-1)\hat{P}_{34}\Big] \\ &= \frac{\rho^3}{2}\frac{1}{\nu}\int d\mathbf{r}_{12}d\mathbf{r}14d\mathbf{r}_{34}\ell(r_{13})\ell(r_{14})\ell(r_{34})\text{CTr}_{1234}\Big[\hat{F}_{12}v_{12}\hat{F}_{12}(\hat{F}_{34}^2-1)\hat{P}_{34}\Big] \\ &= \frac{\rho^2}{2}\int d\mathbf{r}_{12}d\mathbf{r}_{34}\ell(r_{34})^2\text{CTr}_{1234}\Big[\hat{F}_{12}v_{12}\hat{F}_{12}(\hat{F}_{34}^2-1)\hat{P}_{34}\Big]\,. \end{aligned} \tag{202}$$

where in the last line we have used Eq. (199). A change of integration variables leads to

$$v_{4b\to 3b}^{\rm p13} = \frac{\rho^2}{2}\int d\mathbf{r}_{12}d\mathbf{r}_{13}\ell(r_{13})^2 {\rm CTr}_{123}\Big[\hat{F}_{12}v_{12}\hat{F}_{12}(\hat{F}_{13}^2-1)\hat{P}_{13}\Big]\,. \tag{203}$$

The diagram of Fig. 25 can be written as

$$\begin{aligned} v_{4b\to 3b}^{\rm cir} &= -\frac{\rho^4}{A}\int d\mathbf{r}_{1234}\ell(r_{12})\ell(r_{13})\ell(r_{24})\ell(r_{34}){\rm CTr}_{1234}\Big[\hat{F}_{12}v_{12}\hat{F}_{12}(\hat{F}_{34}^2-1)\hat{P}_{12}\hat{P}_{13}\hat{P}_{34}\Big] \\ &= -\frac{\rho^4}{A}\frac{1}{\nu}\int d\mathbf{r}_{1234}\ell(r_{12})\ell(r_{13})\ell(r_{24})\ell(r_{34}){\rm CTr}_{1234}\Big[\hat{F}_{12}v_{12}\hat{F}_{12}(\hat{F}_{34}^2-1)\hat{P}_{12}\hat{P}_{34}\Big] \\ &= -\rho^3\frac{1}{\nu}\int d\mathbf{r}_{12}d\mathbf{r}_{13}d\mathbf{r}_{34}\ell(r_{12})\ell(r_{13})\ell(r_{24})\ell(r_{34}){\rm CTr}_{1234}\Big[\hat{F}_{12}v_{12}\hat{F}_{12}(\hat{F}_{34}^2-1)\hat{P}_{12}\hat{P}_{34}\Big]\,, \end{aligned} \tag{204}$$

having used the fact that only the central term of $(\hat{F}_{34}^2-1)\hat{P}_{34}$ contributes. Since $\ell(r_{24}) = \ell(|\mathbf{r}_{34}-\mathbf{r}_{12}+\mathbf{r}_{13}|)$, exploiting the convolution property of Eq. (199), it turns out that

$$\begin{aligned} v_{4b\to 3b}^{\rm cir} &= -\rho^2\int d\mathbf{r}_{12}d\mathbf{r}_{34}\ell(r_{12})\ell(|\mathbf{r}_{34}-\mathbf{r}_{12}|)\ell(r_{34}){\rm CTr}_{1234}\Big[\hat{F}_{12}v_{12}\hat{F}_{12}(\hat{F}_{34}^2-1)\hat{P}_{12}\hat{P}_{34}\Big] \\ &= -\rho^2\int d\mathbf{r}_{12}d\mathbf{r}_{34}\ell(r_{12})\ell(|\mathbf{r}_{34}-\mathbf{r}_{12}|)\ell(r_{34}){\rm CTr}_{1234}\Big[\hat{F}_{12}v_{12}\hat{F}_{12}(\hat{F}_{34}^2-1)\hat{P}_{34}\hat{P}_{12}\Big] \\ &= -\rho^2\int d\mathbf{r}_{12}d\mathbf{r}_{13}\ell(r_{12})\ell(r_{13})\ell(r_{23}){\rm CTr}_{123}\Big[\hat{F}_{12}v_{12}\hat{F}_{12}(\hat{F}_{13}^2-1)\hat{P}_{13}\hat{P}_{12}\Big]\,. \end{aligned} \tag{205}$$

References

[1] R. B. Wiringa, V. G. J. Stoks, and R. Schiavilla. Accurate nucleon-nucleon potential with charge-independence breaking. *Phys. Rev. C*, 51:38–51, Jan 1995.

[2] M. Piarulli, L. Girlanda, R. Schiavilla, R. Navarro Pérez, J. E. Amaro, and E. Ruiz Arriola. Minimally nonlocal nucleon-nucleon potentials with chiral two-pion exchange including Δ resonances. *Phys. Rev. C*, 91:024003, Feb 2015.

[3] M. Piarulli, L. Girlanda, R. Schiavilla, A. Kievsky, A. Lovato, L. E. Marcucci, Steven C. Pieper, M. Viviani, and R. B. Wiringa. Local chiral potentials with Δ-intermediate states and the structure of light nuclei. *Phys. Rev. C*, 94:054007, Nov 2016.

[4] J. E. Lynn, I. Tews, J. Carlson, S. Gandolfi, A. Gezerlis, K. E. Schmidt, and A. Schwenk. Chiral Three-Nucleon Interactions in Light Nuclei, Neutron-α Scattering, and Neutron Matter. *Phys. Rev. Lett.*, 116:062501, Feb 2016.

[5] B. S. Pudliner, V. R. Pandharipande, J. Carlson, Steven C. Pieper, and Robert B. Wiringa. Quantum Monte Carlo calculations of nuclei with A ¡= 7. *Phys. Rev.*, C56:1720–1750, 1997.

[6] Jun ichi Fujita and Hironari Miyazawa. Pion theory of three-body forces. *Progress of Theoretical Physics*, 17(3):360–365, 1957.

[7] D. R. Hartree. The wave mechanics of an atom with a non-coulomb central field. part i. theory and methods. *Mathematical Proceedings of the Cambridge Philosophical Society*, 24(01):89–110, 1928.

[8] V. Fock. Näherungsmethode zur lösung des quantenmechanischen mehrkörperproblems. *Z. Physik*, 61:126–148, Feb 1930.

[9] J. C. Slater. Note on hartree's method. *Phys. Rev.*, 35:210–211, Jan 1930.

[10] E. Lipparini. *Modern Many-Particle Physics: Atomic Gases, Nanostructures and Quantum Liquids*. World Scientific, 2008.

[11] Maria Goeppert Mayer. On closed shells in nuclei. ii. *Phys. Rev.*, 75:1969–1970, Jun 1949.

[12] Maria Goeppert Mayer. Nuclear configurations in the spin-orbit coupling model. i. empirical evidence. *Phys. Rev.*, 78:16–21, Apr 1950.

[13] Otto Haxel, J. Hans D. Jensen, and Hans E. Suess. On the "magic numbers" in nuclear structure. *Phys. Rev.*, 75:1766–1766, Jun 1949.

[14] A.L. Fetter and J.D. Walecka. *Quantum Theory of Many-Particle Systems*. Dover Books on Physics. Dover Publications, 2003.

[15] Arya Akmal. *Variational studies of nucleon matter with realistic potentials*. PhD thesis, University of Illinois at Urbana-Champaign, 1998.

[16] Robert Jastrow. Many-body problem with strong forces. *Phys.Rev.*, 98:1479–1484, 1955.

[17] John W. Clark. Variational theory of nuclear matter. *Progress in Particle and Nuclear Physics*, 2(0):89 – 199, 1979.

[18] V. R. Pandharipande and R. B. Wiringa. Variations on a theme of nuclear matter. *Rev. Mod. Phys.*, 51:821–861, Oct 1979.

[19] K. A. Brueckner, C. A. Levinson, and H. M. Mahmoud. Two-body forces and nuclear saturation. i. central forces. *Phys. Rev.*, 95:217–228, Jul 1954.

[20] K. A. Brueckner. Nuclear saturation and two-body forces. ii. tensor forces. *Phys. Rev.*, 96:508–516, Oct 1954.

[21] K. A. Brueckner and C. A. Levinson. Approximate reduction of the many-body problem for strongly interacting particles to a problem of self-consistent fields. *Phys. Rev.*, 97:1344–1352, Mar 1955.

[22] K. A. Brueckner. Many-body problem for strongly interacting particles. ii. linked cluster expansion. *Phys. Rev.*, 100:36–45, Oct 1955.

[23] H. A. Bethe. Nuclear many-body problem. *Phys. Rev.*, 103:1353–1390, Sep 1956.

[24] J. Goldstone. Derivation of the Brueckner Many-Body Theory. *Royal Society of London Proceedings Series A*, 239:267–279, February 1957.

[25] H. Müther and A. Polls. Two-body correlations in nuclear systems. *Progress in Particle and Nuclear Physics*, 45(1):243 – 334, 2000.

[26] M Baldo and C Maieron. Equation of state of nuclear matter at high baryon density. *Journal of Physics G: Nuclear and Particle Physics*, 34(5):R243, 2007.

[27] K. Hebeler and A. Schwenk. Chiral three-nucleon forces and neutron matter. *Phys. Rev. C*, 82:014314, Jul 2010.

[28] K. Hebeler and R. J. Furnstahl. Neutron matter based on consistently evolved chiral three-nucleon interactions. *Phys. Rev. C*, 87:031302, Mar 2013.

[29] C. Drischler, K. Hebeler, and A. Schwenk. Asymmetric nuclear matter based on chiral two- and three-nucleon interactions. *Phys. Rev. C*, 93:054314, May 2016.

[30] E. Feenberg. *Theory of quantum fluids*. Pure and applied physics. Academic Press, 1969.

[31] C.A. Croxton. *Progress in liquid physics*. Wiley-Interscience Publication. Wiley, 1978.

[32] M. H. Kalos, Michael A. Lee, P. A. Whitlock, and G. V. Chester. Modern potentials and the properties of condensed ^{4}He. *Phys. Rev. B*, 24:115–130, Jul 1981.

[33] Q. N. Usmani, S. Fantoni, and V. R. Pandharipande. Three-body correlations in liquid ^{4}He. *Phys. Rev. B*, 26:6123–6130, Dec 1982.

[34] Saverio Moroni, Stefano Fantoni, and Gaetano Senatore. Euler Monte Carlo calculations for liquid ^{4}He and ^{3}He. *Phys. Rev. B*, 52:13547–13558, Nov 1995.

[35] R. P. Feynman and Michael Cohen. Energy spectrum of the excitations in liquid helium. *Phys. Rev.*, 102:1189–1204, Jun 1956.

[36] O. Benhar, V. R. Pandharipande, and Steven C. Pieper. Electron-scattering studies of correlations in nuclei. *Rev. Mod. Phys.*, 65:817–828, Jul 1993.

[37] Vijay R. Pandharipande, Ingo Sick, and Peter K. A. deWitt Huberts. Independent particle motion and correlations in fermion systems. *Rev. Mod. Phys.*, 69:981–991, Jul 1997.

[38] John W. Clark and Paul Westhaus. Method of correlated basis functions. *Phys. Rev.*, 141:833–857, Jan 1966.

[39] Stefano Fantoni and Adelchi Fabrocini. Correlated basis function theory for fermion systems. In Jesùs Navarro and Artur Polls, editors, *Microscopic Quantum Many-Body Theories and Their Applications*, volume 510 of *Lecture Notes in Physics*, pages 119–186. Springer Berlin / Heidelberg, 1998. 10.1007/BFb0104526.

[40] Russell H. Kullas and William J. Mullin. Theory of dilute solutions of ^{3}He in superfluid ^{4}He. i. perturbation theory in a nonorthogonal basis. *Journal of Low Temperature Physics*, 11:301–319, 1973. 10.1007/BF00656555.

[41] P.M.C. Morse and H. Feshbach. *Methods of theoretical physics*. Number pt. 2 in International series in pure and applied physics. McGraw-Hill, 1953.

[42] John W. Clark and Eugene Feenberg. Simplified treatment for strong short-range repulsions in n-particle systems. i. general theory. *Phys. Rev.*, 113:388–399, Jan 1959.

[43] S. Fantoni. Linked-cluster perturbative expansion in correlated-basis theory. *Phys. Rev. B*, 29:2544–2550, Mar 1984.

[44] J.W. Clark, P.M. Lam, and W.J. Ter Louw. Perturbation corrections to the jastrow energy for simple models of nuclear matter. *Nuclear Physics A*, 255(1):1 – 12, 1975.

[45] A.D. Jackson, E. Krotscheck, D.E. Meltzer, and R.A. Smith. Landau parameters and pairing-on the shores of the nuclear fermi sea. *Nuclear Physics A*, 386(1):125 – 165, 1982.

[46] B. L. Friman and E. Krotscheck. Zero sound, spin fluctuations, and effective mass in liquid ^{3}He. *Phys. Rev. Lett.*, 49:1705–1708, Dec 1982.

[47] V.R. Pandharipande. Dense neutron matter with realistic interactions. *Nuclear Physics A*, 174(3):641 – 656, 1971.

[48] M. L. Ristig, W. J. Ter Louw, and J. W. Clark. Tensor correlations in nuclear matter. *Phys. Rev. C*, 3:1504–1513, Apr 1971.

[49] V.R. Pandharipande. Variational calculation of nuclear matter. *Nuclear Physics A*, 181(1):33 – 48, 1972.

[50] I.E. Lagaris and V.R. Pandharipande. Variational calculations of ?8 models of nuclear matter. *Nuclear Physics A*, 334(2):217 – 228, 1980.

[51] S. Fantoni and V.R. Pandharipande. Correlated basis theory of nuclear matter response functions. *Nuclear Physics A*, 473(2):234 – 266, 1987.

[52] A. Fabrocini and S. Fantoni. Microscopic calculation of the longitudinal response of nuclear matter. *Nuclear Physics A*, 503(2):375 – 403, 1989.

[53] Omar Benhar, Adelchi Fabrocini, and Stefano Fantoni. The nucleon spectral function in nuclear matter. *Nuclear Physics A*, 505(2):267 – 299, 1989.

[54] O. Benhar, A. Fabrocini, and S. Fantoni. Nuclear-matter green functions in correlated-basis theory. *Nuclear Physics A*, 550(2):201 – 222, 1992.

[55] J. Carlson, S. Gandolfi, F. Pederiva, Steven C. Pieper, R. Schiavilla, K. E. Schmidt, and R. B. Wiringa. Quantum Monte Carlo methods for nuclear physics. *Rev. Mod. Phys.*, 87:1067, 2015.

[56] Per-Olov Löwdin. On the non-orthogonality problem connected with the use of atomic wave functions in the theory of molecules and crystals. *The Journal of Chemical Physics*, 18(3):365–375, 1950.

[57] S. Fantoni and V. R. Pandharipande. Orthogonalization of correlated states. *Phys. Rev. C*, 37:1697–1707, Apr 1988.

[58] S. Fantoni and S. Rosati. Jastrow correlations and an irreducible cluster expansion for infinite boson or fermion systems. *Nuovo Cimento A Serie*, 20:179–193, March 1974.

[59] S. Fantoni and S. Rosati. The hypernetted-chain approximation for a fermion system. *Nuovo Cimento A Serie*, 25:593–615, February 1975.

[60] E. Krotscheck and M.L. Ristig. Long-range jastrow correlations. *Nuclear Physics A*, 242(3):389 – 405, 1975.

[61] V.R. Pandharipande and R.B. Wiringa. A variational theory of nuclear matter. *Nuclear Physics A*, 266(2):269 – 316, 1976.

[62] Mayer Joseph Edward and Mayer Maria Goeppert. *Statistical mechanics*. J. Wiley & Sons; Chapman & Hall, New York; London, 1940.

[63] F. Arias de Saavedra, C. Bisconti, G. CoÕ, and A. Fabrocini. Renormalized fermi hypernetted chain approach in medium-heavy nuclei. *Physics Reports*, 450(1-3):1 – 95, 2007.

[64] J. Morales, V. R. Pandharipande, and D. G. Ravenhall. Improved variational calculations of nucleon matter. *Phys. Rev. C*, 66:054308, Nov 2002.

[65] S. Fantoni and S. Rosati. Calculation of the two-body correlation function for fermion systems. *Lettere Al Nuovo Cimento (1971-1985)*, 10:545–551, 1974. 10.1007/BF02784779.

[66] E. Krotscheck and M.L. Ristig. Hypernetted-chain approximation for dense fermi fluids. *Physics Letters A*, 48(1):17 – 18, 1974.

[67] J.M.J. van Leeuwen, J. Groeneveld, and J. de Boer. New method for the calculation of the pair correlation function. i. *Physica*, 25(7-12):792 – 808, 1959.

[68] S. Fantoni and K.E. Schmidt. Fermi hypernetted chain calculations in a periodic box. *Nuclear Physics A*, 690(4):456 – 470, 2001.

[69] E. Manousakis, S. Fantoni, V. R. Pandharipande, and Q. N. Usmani. Microscopic calculations for normal and polarized liquid ^{3}He. *Phys. Rev. B*, 28:3770–3781, Oct 1983.

[70] B. Wiringa. Elementary diagrams in nuclear matter. private communication, 2007.

[71] V. R. Pandharipande and H. A. Bethe. Variational method for dense systems. *Phys. Rev. C*, 7:1312–1328, Apr 1973.

[72] Fumiaki Iwamoto and Masami Yamada. Cluster development method in the quantum mechanics of many particle system, i. *Progress of Theoretical Physics*, 17(4):543–555, 1957.

[73] R.B. Wiringa and V.R. Pandharipande. A variational theory of nuclear matter (iii). *Nuclear Physics A*, 317(1):1 – 22, 1979.

[74] I.E. Lagaris and V.R. Pandharipande. Variational calculations of realistic models of nuclear matter. *Nuclear Physics A*, 359(2):349 – 364, 1981.

[75] S. Kirkpatrick, C.D. Gelatt, and M.P. Vecchi. Optimization by Simulated Annealing. *Science*, 220:671–680, 1983.

[76] B.H. Bransden and C.J. Joachain. *Physics of Atoms and Molecules*. Pearson Education. Prentice Hall, 2003.